Materials Research Express

TOPICAL REVIEW

Synergy of physical properties of low-dimensional carbon-based systems for nanoscale device design

RECEIVED
1 November 2018

REVISED
8 December 2018

ACCEPTED FOR PUBLICATION
28 December 2018

PUBLISHED
16 January 2019

N A Poklonski[1,4], S A Vyrko[1], A I Siahlo[1], O N Poklonskaya[1], S V Ratkevich[1], N N Hieu[2,4] and A A Kocherzhenko[3]

[1] Physics Department, Belarusian State University, Nezavisimosti Ave 4, Minsk 220030, Belarus
[2] Institute of Research and Development, Duy Tan University, Da Nang, Viet Nam
[3] California State University, East Bay, 25800 Carlos Bee Blvd, Hayward, CA 94542, United States of America
[4] Authors to whom any correspondence should be addressed.

E-mail: poklonski@bsu.by and hieunn@duytan.edu.vn

Keywords: Low-dimensional carbon structures, fullerenes, nanotubes, graphene, tunnel diode, point defects in diamond, nanoelectromechanical systems

Abstract

We review the principles of formation, physical properties, and current or envisaged applications for a wide range of carbon allotropic forms. We discuss experimental and theoretical advances relating to staple zero-, one-, and two-dimensional carbon structures, such as fullerenes, carbon nanotubes, and graphene. In addition we emphasize research on emerging carbon allotropes (carbon nanoscrolls, funnels, etc) that result from combining or deforming allotropic forms with well-defined dimensionality. Such materials fall in-between clearly delineated dimensional categories and consequently exhibit unique characteristics that are promising for electronic, optical, and mechanical applications. We also consider other approaches to tuning properties of carbon-based materials, such as chemical functionalization, intentional introduction of structural disorder, and placement of guest atoms or molecules inside hollow structures. Finally, we discuss the properties of and experimental methods for studying zero-dimensional systems (paramagnetic nitrogen impurity atoms) in diamond matrix. The review emphasizes the interplay between the various material properties of carbon-based nanostructures and the designs for nanoscale devices that rely on synergistic combinations of these properties. For example, an electromechanical vibrator, a strain sensor, a nanodynamometer, and a nanoelectromechanical memory cell that we describe exploit both electronic and nanomechanical properties of low-dimensional carbon structures, a reed switch and a magnetic field sensor use magnetic and nanomechanical properties, a maser based on nitrogen-doped diamond uses thermal and optoelectronic properties, etc. All presented device concepts have been validated by calculations, and some have been implemented experimentally.

1. Introduction

Production of low-dimensional systems, research on their physical, chemical, and biological properties, and technological innovations that they foster are of great significance to engineering [1–3]. This article provides an overview of theoretical and experimental studies on the physical properties of low-dimensional carbon materials, and of devices based on them. We briefly review results and associated hypotheses and discuss the outlook for future research on low-dimensional carbon systems, particularly emphasizing the potential for synergistically combining their various properties in the design of nanoscale devices.

We start by defining the terminology used in the text and illustrations [4–6]: allotropy, nanotechnology, low-dimensional systems, and nanomaterials.

Allotropy is the existence of two or more distinct structural forms with different properties for a given chemical element in the same state of matter. The term allotropy only applies to homoatomic substances (e.g., carbon), regardless of their state. In contrast, the term 'polymorphism' has a similar meaning but only refers to

solids, whether homoatomic or heteroatomic. The terms 'allotropy' and 'polymorphism' are thus synonymous for homoatomic solids (e.g., white and red phosphorus, gray and white tin, graphite and diamond).

Nanotechnology refers to the production, characterization methods, and applications of structures with characteristic sizes ranging from about 0.1 nm to 100 nm. Varying the size, shape, and relative positioning of nanostructures, even while maintaining their chemical composition, allows control over their properties, such as the melting point, solubility or transparency. Nanoscale structures can be produced from bulk materials using *top-down* approaches, such as ablation (the removal of a surface layer of a solid exposed to laser radiation [7–9] and/or plasma flux [10]) and selective removal of atoms from multicomponent compounds by ion [11] or electron beams [12]. Alternatively, nanoscale structures can be assembled from single atoms using *bottom-up* approaches, such as selective transfer of atoms from a probe tip of a scanning probe microscope onto a surface (approaching self-assembled structures with optimal design [13]) or chemical synthesis of atomically precise structures [14, 15].

Low-dimensional systems are consolidated systems of many particles with dimensions in at least one spatial direction that are comparable to the characteristic lengths for states and/or processes in the system (see, e.g., [16]). Examples of such characteristic lengths are the mean free path of a particle between scattering, recombination, or decay events and the average de Broglie wavelength of a particle.

Quantum confinement of (quasi)particles in one, two or three directions modifies the dependence of their energy on the (quasi)momentum [17] and spin (or intrinsic dipole magnetic moment of the particle) in the quantization direction. If this energy quantization occurs in all three directions, the system is called *zero-dimensional*. If the energy quantization occurs in two directions and free motion occurs in one direction, the system is called *one-dimensional*. If the energy quantization occurs in one direction and free motion occurs in two directions, the system is called *two-dimensional*. Examples of zero-dimensional systems are fullerenes [18], atomic clusters, quantum dots [19], and atomic point defects in a crystalline matrix. Examples of one-dimensional systems are carbyne (a chain of carbon atoms) [4, 20], carbon nanotubes [21], quantum threads, and ion tracks in diamond [22]. Examples of two-dimensional systems are graphene [23], as well as surfaces, interfaces, and stacking faults of atomic planes in a crystal. Low-dimensional systems can also be *fractal* (have fractional dimensionality) [24].

Based on the time-dependence of the effect that produces quantum confinement, low-dimensional systems can be classified as either *stationary* or *non-stationary*. Stationary low-dimensional systems include semiconductor super-lattices that consist of crystalline layers with different chemical composition, crystallographic orientation or structure and have a spatial periodicity in one direction that is smaller than the mean free path of electrons and/or holes [25]. Non-stationary low-dimensional systems include solitons, domains of the electric field in Gunn diodes [26], current pinches in doped crystalline semiconductors [27], and sprays of light in photorefractive crystals [28].

Materials that are comprised of low-dimensional systems are referred to as *nanostructured* materials, or simply *nanomaterials*. Such materials are built from atomic clusters, granules, nanoscale pores (conventionally with sizes from about 1 nm to 100 nm) in a solid matrix, fibers, tubes, layers, etc. The properties of nanostructured materials are distinct from those of uniform materials with the same chemical composition [2, 29].

Agglomeration of carbon atoms can lead to the formation of diverse allotropic forms that are stable under certain conditions [4, 30–32]. The variety of these structures is schematically shown in figure 1. Carbon also forms a remarkable variety of heteroatomic compounds: notably, it is the defining component of all organic materials. Such chemical ubiquity is a consequence of carbon's ability to readily change the type of hybridization of its valence orbitals in the process of forming both C–C bonds and bonds with atoms of other chemical elements (primarily hydrogen, oxygen, iron, silicon, nitrogen, and boron).

Changes in the valence of atoms depending on their environment often lead to dramatic changes in the physical properties of materials. For example, three-dimensional bulk materials can be mechanically reinforced with fractal systems [33, 34]. Electrical properties of materials can also be altered. For instance, the passivation of graphene on both sides with hydrogen leads to the formation of graphane, the two-dimensional counterpart of diamond with sp^3-hybridized carbon atoms. Unlike graphene that is highly electrically conductive, graphane is a dielectric at room temperature. Reversing the conversion of graphane to graphene by annealing recovers the electrical conductivity [35].

In this paper we explore the vast landscape of carbon-based materials across dimensionalities. We review experimental and theoretical research on staple low-dimensional carbon structures, such as fullerenes, carbon nanotubes, and graphene. However, many promising carbon allotropes fall in-between clearly delineated dimensional categories. For example, carbon nanoscrolls are two-dimensional (2D) graphene sheets rolled into one-dimensional (1D) spirals. They share some properties with 1D and others with 2D materials, as well as exhibit unique characteristics that are not typical of either dimensionality. Combining or deforming allotropic forms with well-defined dimensionality often results in such structures. They present a new frontier in

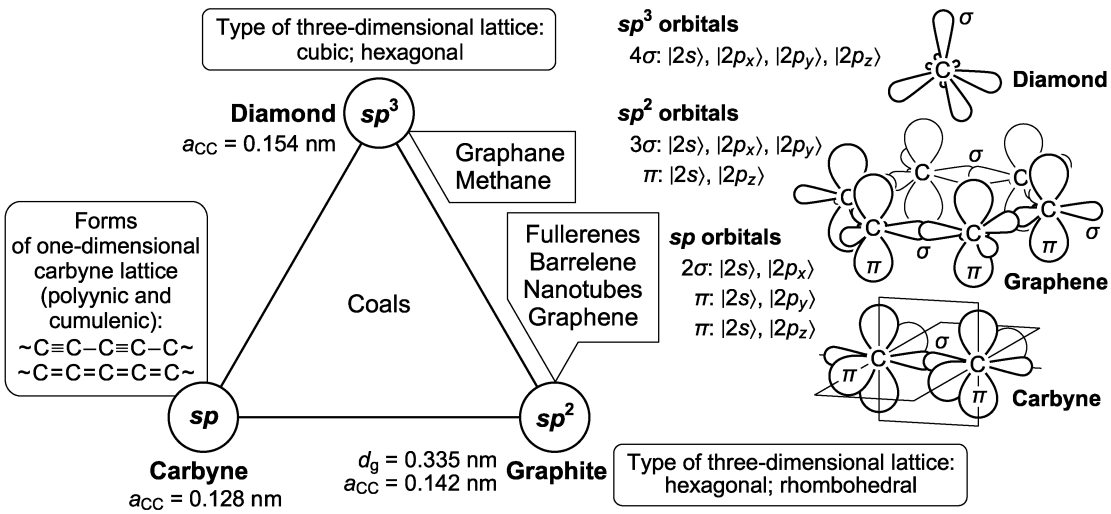

Figure 1. Allotropes of carbon associated with changes in the hybridization of valence orbitals. Here a_{CC} is the distance between nearest atoms, d_g is the distance between atomic planes (graphene) in graphite, σ and π are the hybrid orbitals of carbon atoms. (Graphane and methane are compounds composed of carbon and hydrogen.)

customization of carbon-based materials, and we emphasize interrelations between them and more traditional carbon allotropes. We also consider other approaches to tuning properties of carbon-based materials, such as chemical functionalization, intentional introduction of structural disorder, and placement of guest atoms or molecules inside hollow structures.

To give a broad perspective of the field, we review the principles of formation, physical properties, as well as current or envisaged applications for a wide range of carbon allotropic forms. Our primary focus is on electrical, magnetic, and nanomechanical properties that are particularly sensitive to the dimensionality of the carbon based material. We emphasize the interplay between these material properties and discuss how their various combinations enable the design of novel nanoscale devices. All presented device concepts have been validated by calculations, and some have been implemented experimentally.

2. Zero-dimensional systems

Since their discovery (in 1985) [18], fullerenes and their derivatives have commanded ever-increasing attention from scientists and engineers [36, 37]. A variety of fullerenes and related low-dimensional systems exist; approaches to their classification are described in [38]. Multiple applications for these materials emerged in recent years, including as photosensitizers in photodynamic therapy [39, 40], as catalysts in fuel cells [41, 42], and as electron acceptors in organic blend photovoltaics [43–45]. In donor-acceptor systems, fullerenes and their derivatives often ensure more efficient electron-hole separation than other acceptors due to their high density of unoccupied states close in energy to the lowest unoccupied orbitals of organic donors [46, 47]. Fullerenes also have catalytic properties. Small concentrations of a mixture of fullerenes C_{60}–C_{70} (up to 0.255 wt%) in the graphite feed material lower the activation energy of the phase transition from graphite to diamond by a factor of 1.6 (for synthesis carried out in the temperature range of 1600–1800 K at a pressure of 5 GPa with Ni–Mn as metal catalysts) [48].

Industrial-scale production of low-cost carbon nanostructures for applications requires a theoretical understanding of the mechanisms of their formation and growth [49, 50]. Currently, the most widely accepted model of fullerene formation is the 'fullerene road' [51] (see figure 2(a)). In this model, carbon clusters of 30 to 40 atoms can become fullerenes, then grow into larger fullerenes by a series of C_2 insertions. An evident weakness of this model is that it does not explain the formation of small fullerenes. However, experiments confirm the existence of the smallest possible fullerene, C_{20} [52], therefore the mechanism of its formation needs to be investigated. Understanding this mechanism is particularly important because C_{20} could mediate the formation of larger fullerenes and serve as a nucleation center for carbon nanotubes.

A possible pathway for C_{20} formation and its subsequent growth into larger fullerenes and carbon nanotubes is shown in figure 2(b) [53].

Two isomers consisting of ten carbon atoms, C_{10}^{rg} rings and C_{10}^{st} stars, can be formed in carbon plasma. Density functional theory (DFT) calculations with the hybrid exchange-correlation energy functional UB3LYP and the 6-31G(d,p) basis set show that the C_{10}^{st} isomer is metastable. Its ground state energy is 10.33 eV above

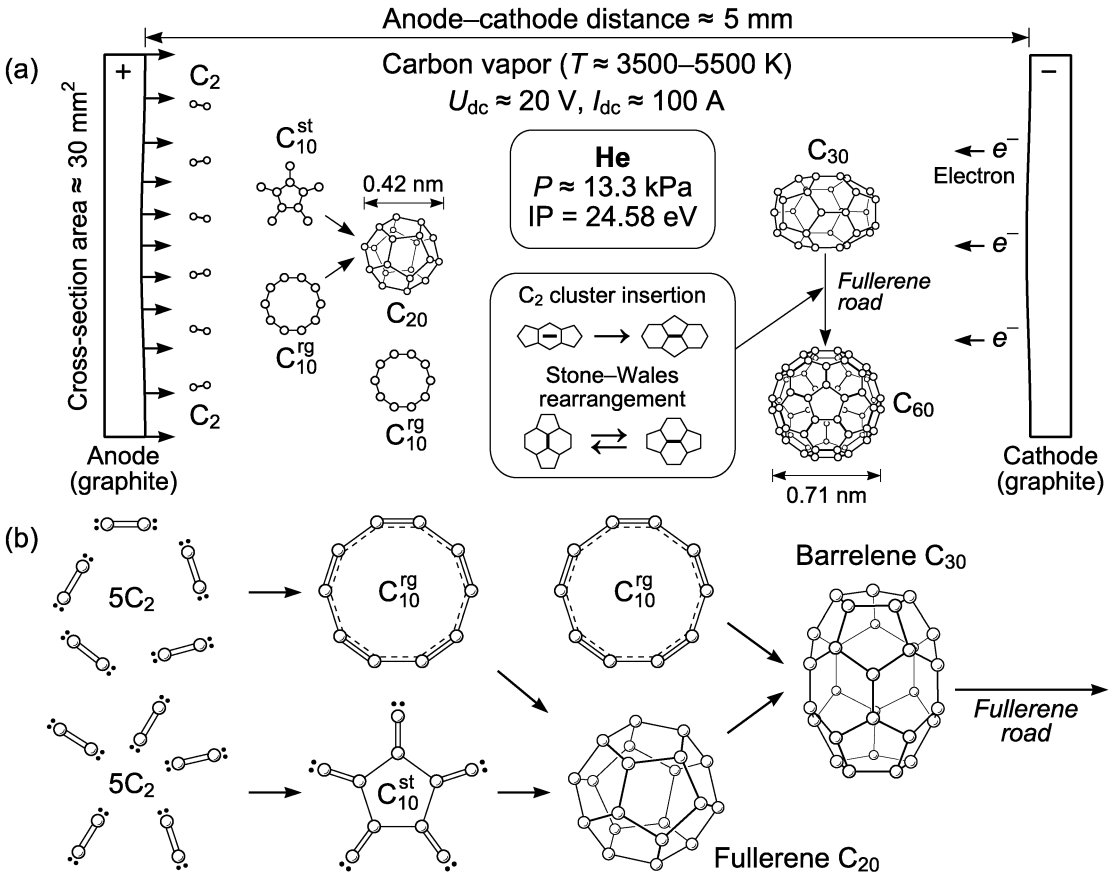

Figure 2. Scheme of the fullerene formation in the carbon plasma (a) and a possible pathway for the creation of the C_{20} and C_{30} molecules (b) adapted from [53]. A typical cross-section of disc-shaped graphite electrodes is about 30 mm^2; U_{dc} is the DC voltage, I_{dc} is the direct current, T is the plasma temperature, P is the partial pressure of helium, and IP is the ionization potential of He atoms. Dots next to carbon atoms represent the valence electrons that are not involved in the formation of C–C bonds.

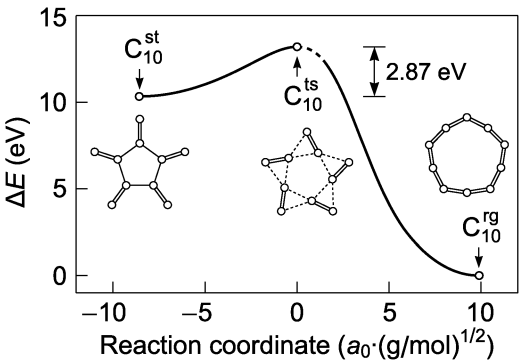

Figure 3. Reaction coordinate for the $C_{10}^{st} \rightarrow C_{10}^{ts} \rightarrow C_{10}^{rg}$ transformation, where ΔE is the total electronic energy of the molecule relative to the C_{10}^{rg} ground state; a_0 is the Bohr radius; adapted from [53]. The configurations of the C_{10} isomers are shown near the corresponding section of the graph. Dotted lines in the C_{10}^{ts} transition state configuration indicate breaking and forming bonds. The dotted section in the graph corresponds to intermediate configurations with breaking and forming bonds.

that of the C_{10}^{rg} isomer, and the barrier for the isomeric transition $C_{10}^{st} \rightarrow C_{10}^{rg}$ is 2.87 eV (figure 3). Despite the very high energy barrier, this isomeric transition retains the five-fold symmetry axis. (For comparison, the barrier for nitrogen inversion in the ammonia molecule that retains its symmetry is 0.2 eV [54].)

The formation of the C_{20} fullerene in carbon plasma can then occur by several mechanisms. Calculations show that the most probable is the fusion of two C_{10}^{st} star isomers. The fusion of a C_{10}^{rg} ring and a C_{10}^{st} star can also occur at temperatures $T < 3100$ K. The fusion of two C_{10}^{rg} rings is much less probable, but can occur at $T < 800$ K. It follows that the formation of C_{20} is most efficient when large numbers of C_{10}^{st} star isomers are present in the carbon plasma. Therefore, the presence of hydrogen in the carbon plasma or ultraviolet

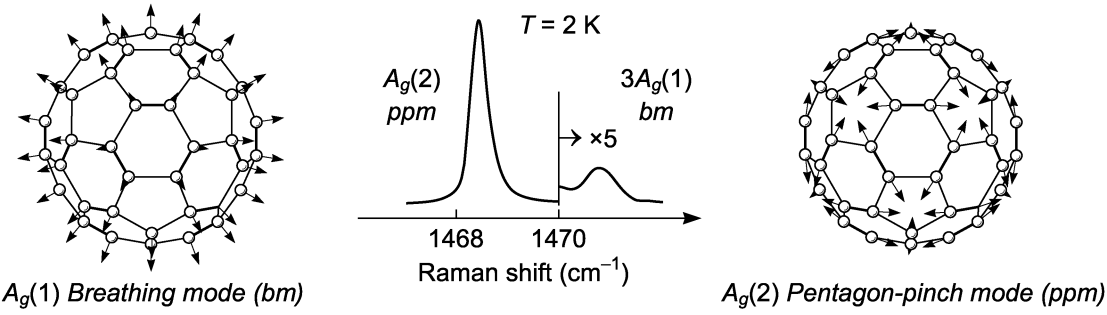

Figure 4. Raman scattering data for totally symmetric vibrations $A_g(2)$, $3A_g(1)$ of the fullerene C_{60} and corresponding motion of carbon atoms indicated by arrows. The fine structure on the right shoulder of the $A_g(2)$ peak occurs due to the Fermi resonance (the interaction between vibrational modes due to their anharmonicity) between the *ppm* vibration $A_g(2)$ and the second overtone $3A_g(1)$ of the *bm* vibration $A_g(1)$. (Photon with wavenumber 1 cm^{-1} in vacuum has energy 0.124 meV.)

irradiation that facilitate the $C_{10}^{st} \rightarrow C_{10}^{rg}$ transition are expected to inhibit C_{20} formation. Further, the formation of the C_{30} fullerene can occur by confluence of C_{10}^{rg} (or C_{10}^{st}) with the C_{20} carbododecahedron.

Modeling configurational transitions in atomic clusters is challenging [55], particularly because both spontaneous and induced point symmetry breaking are common in low-dimensional systems [56, 57]. For example, the analogue of the dynamic Jahn–Teller effect was computationally discovered in the dication carbododecahedron C_{20}^{2+} [58]. The ground state of C_{20}^{2+} has $\boldsymbol{D}_3$-symmetry that is manifested in the infrared vibrational spectrum. This is a case of $\boldsymbol{I}_h$-symmetry breaking (lowering to $\boldsymbol{D}_3$) due to the repulsion of uncompensated positive charges on the carbon atoms (Coulomb distortion). Such effects can be crucial for chemical transformations among fullerenes, particularly in highly charged states. For instance, the lowest-energy isomer of highly charged C_{60} is not the spherical buckyball, but an elongated barrelene that can undergo fission with the emission of C_{20}^{2+} [59].

Calculations using DFT and second-order Møller–Plesset perturbation theory predict the fullerenes to be lowest energy conformations for carbon systems with more than 20 atoms [60–62]. The upper size limit for thermodynamically stable fullerenes or multishell fullerenes (carbon onions) has been predicted to be ~1000 atoms [63, 64]. The thermodynamics and kinetics of large fullerene formation from a variety of starting materials including carbon vapor [65–68], carbon nanotubes [69], graphene flakes [70], nanodiamond [71], and amorphous carbon clusters [72] are actively studied using molecular dynamics.

Symmetry and symmetry breaking are responsible for many properties of fullerenes and of materials composed of them. For instance, computational studies of C_{60} [73] in conjunction with Raman scattering experiments on fullerites [74] suggest the possibility of the Fermi resonance (the interaction between vibrational modes due to their anharmonicity) for two totally symmetric vibrational modes [75] (figure 4). Fullerites (crystalline form of fullerene) that contain atoms of metals in their crystallographic voids are called fullerides. C_{60} fullerides with K, Rb, Cs, Ga, In, Sn or Bi atoms posses superconducting properties (temperature of transition to superconducting state up to 33 K) [76, 77].

Most current applications of fullerenes involve bulk materials, but prospects of using single fullerenes in single-molecule electronic devices are particularly intriguing [78–80]. In single-molecule electronics, fundamentally non-classical effects that occur at the molecular level, such as Coulomb blockade [78], Franck–Condon blockade [79], or constructive and destructive interference of the electronic wavefunction [81] are used to control electrical current. Molecular electronic devices range from current rectifiers [82–85] to transistors [86, 87] (see also figure 5).

In single-fullerene transistors, a molecule such as C_{60} [88, 89] or C_{140} [90], is placed in a nanoscale gap between metal electrodes created, e.g., by electromigration [91]. The fullerene is electronically coupled to the electrodes, allowing for quantized single-electron tunneling current in the system that can be controlled by a gate electrode. A possible design of a C_{20}-based molecular triode is shown in figure 5. As seen in that figure, changing the positioning of the fullerene molecule in the gap can control the current-voltage characteristic of the device. The well-defined size and high chemical stability of fullerenes can lead to improved device performance relative to, e.g., single-electron transistors based on semiconducting nanocrystals [92].

Fullerene-based single-molecule devices show promise for applications in quantum information processing [93, 94]. Superconducting correlations, a prime example of electronic phase coherence phenomena that are employed in quantum computing, have been observed for fullerenes both in ungated junctions [95] and in transistors [89]. Qubit realizations based on endohedral fullerenes containing heteroatoms with long spin lifetimes inside the fullerene cage [96, 97] have been proposed [98, 99]. Endohedral fullerenes containing atoms of ferromagnetic metals (e.g., Fe, Co, Gd) are of particular interest, due to their large magnetic moments. For

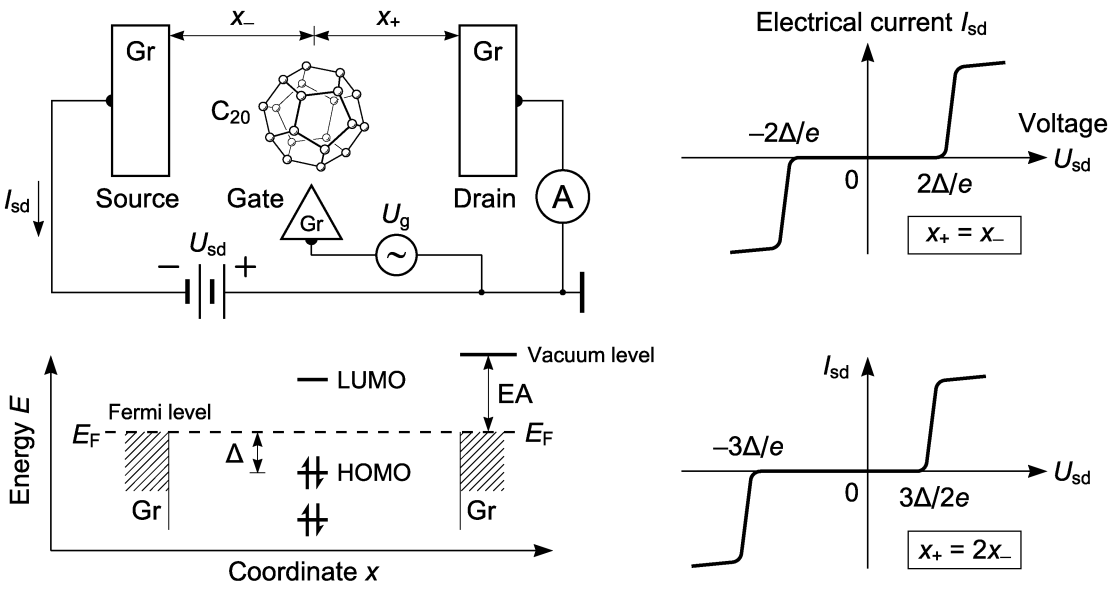

Figure 5. Left: Design of a molecular triode based on a fixed C_{20} molecule between multi-layer graphene (Gr) as electrodes and the corresponding electron energy diagram $E(x)$. Right: current–voltage characteristics for equal ($x_+ = x_-$) and different ($x_+ = 2x_-$) distances of molecule to source and drain at the gate voltage $U_g = 0$ at low temperatures. I_{sd} is the source–drain direct current, U_{sd} is the source–drain voltage, Δ is the gap between Fermi level E_F and HOMO of C_{20} molecule (HOMO is the highest occupied molecular orbital and LUMO is the lowest unoccupied molecular orbital), EA is the electron affinity for electrodes; EA $> 3\Delta$; e is the elementary charge.

instance, quantum chemical calculations reveal that the smallest magnetic endofullerene Fe@C_{20} has a septet ground state and a magnetic moment of about 8 Bohr magneton [100].

3. One-dimensional systems

The formation of carbon filaments in the process of thermal decomposition of methane has been reported as early as 1889, and in 1952 transmission electron microscopy supplied evidence that such filaments could have tubular structure [101–103]. However, these carbon allotropes, now called nanotubes, only attracted widespread attention in the early 1990s, after S Iijima published a report on their synthesis in *Nature* [21]. At the time, the recent discovery of fullerenes prompted researchers to seek out other structures that can be formed by folding graphitic carbon sheets. Carbon nanotubes (CNTs) are one-dimensional systems that are closely related to fullerenes. Ever since, CNTs have been extensively studied and applied due to their remarkable mechanical, physical, and chemical properties [104–106].

The highest mean fracture strength of any materials (>100 GPa) has been reported for CNTs [107]. Because of such extraordinary strength, CNTs can have length-to-diameter aspect ratios greater than 10^8, well above those of any other material [108]. Therefore, CNT properties are typically strongly anisotropic. For instance, materials based on them can have excellent heat conductivity at room temperature (about an order of magnitude greater than copper) along the tubes [109], but be heat insulators in the lateral direction. The optoelectronic properties of CNTs are also anisotropic and are determined by the nanotube topology: depending on it the CNT may be metallic or semiconducting [110]. Superconducting CNTs have also been reported [111, 112].

CNTs that spontaneously form in the vapor-phase deposition of carbon [21, 113] are predominantly multi-walled (MWCNTs): that is, they consist of several coaxial carbon cylinders of varying diameter. However, single-walled carbon nanotubes (SWCNTs) can be obtained using arc discharge evaporation of a carbon electrode with a metal catalyst [114–116] or by laser ablation [117]. (A similar method is also used for growing crystalline silicon nanowires [118, 119].) SWCNTs are of particular interest in nanotechnology due to their well-defined and controllable properties.

SWCNTs are denoted by two indices (n, m) that determine their chiral vector: $\mathrm{C}(n,\ m) = n\mathbf{a}_1 + m\mathbf{a}_2$, where n and m are natural numbers including zero, $\mathbf{a}_1$ and $\mathbf{a}_2$ are the basis vectors of the hexagonal graphene lattice. There are two ways to define the direction of the $\mathbf{a}_2$ vector. The use of a 60° angle between basis vectors is commonly accepted. When the graphene plane is rolled into a nanotube, the beginning and the end of the chiral vector are 'glued' together (figure 6). CNTs that have indices (n, 0) are called *zigzag*, CNTs that have indices (n, n) are called *armchair*, and CNTs that have indices (n, m) with $n \neq m$ and $m \neq 0$ are called *chiral*. To ensure that the same structure is not labeled in two different ways, index m is taken in the range $-n/2 < m \leqslant n$. Nanotubes

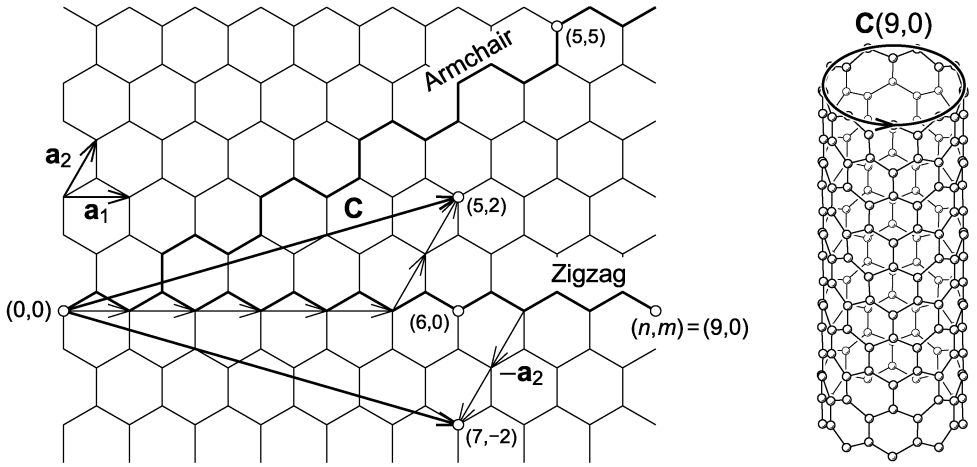

Figure 6. Scheme of rolling a single-walled carbon nanotube defined by chiral vector $\mathbf{C}(n, m) = n\mathbf{a}_1 + m\mathbf{a}_2$ from a graphene strip; $\mathbf{a}_1$ and $\mathbf{a}_2$ are the basis vectors of the hexagonal graphene lattice. Chiral vectors of mirror symmetric metallic nanotubes (5, 2) and (7, −2) are shown. SWCNT diameter is $d = |\mathbf{C}|/\pi$, where $|\mathbf{C}| = a\sqrt{n^2 + m^2 + nm}$; $a = |\mathbf{a}_1| = |\mathbf{a}_2| = a_{CC}\sqrt{3} = 0.246$ nm; the distance between the nearest carbon atoms in the graphene layer is $a_{CC} = 0.142$ nm. Diameter of zigzag SWCNT (9, 0) is ≈0.71 nm.

(n, m) and $(n + m, -m)$ are mirror images of each other. The chiral vector of a nanotube largely determines its electrical properties: in the simple zone folding approximation all armchair CNTs and CNTs that have indices such that $n - m$ is a multiple of 3 are metallic, whereas other CNTs are semiconducting [110, 120–122]. However, the nanotube's curvature, as well as mechanical deformation or the presence of impurities, can significantly affect their conductivity [110, 123, 124]. Under uniaxial strain, pristine armchair CNTs remain metallic [125], but a small band gap that varies linearly with stress opens for zigzag CNTs [126]. In the presence of torsional strain, all CNTs become semiconducting; armchair CNTs are particularly sensitive to such strain [125].

As is generally the case in solid state physics, the band structure of CNTs can be calculated either starting from the free-electron or from the tight-binding approximation [127]. For instance, in the free electron approximation a model of the electronic structure of SWCNTs that takes into account the finiteness of the carbon skeleton thickness has been developed [128]. However, studies of the effects of strain on electronic structure and of interactions between the electronic subsystem and vibrational modes predominantly employ tight-binding models [129, 130].

Within a tight-binding model for the electronic spectrum of armchair SWCNTs it was shown [131] that at liquid helium temperature the rate of energy transfer from the lattice conduction electrons to the CNT frame is determined by the interaction of π electrons with the twiston mode of the phonon spectrum. Calculations demonstrated the possibility of creating a bolometer based on these metallic CNTs, with a thermal time constant of about a microsecond.

As one-dimensional systems, CNTs are subject to Peierls distortions that can cause significant changes to their electronic properties, including a metal–insulator transition that occurs if an energy gap opens at the Fermi level [129, 132–135]. Although the π-electron contribution to the elastic energy of a CNT is relatively small compared to that of the σ electrons, the extended π system is largely responsible for Peierls distortions [132]. It has been predicted that dimerization of the C–C bonds occurs in single-walled carbon nanotubes, leading to quantitative estimates of the Peierls distortions [133].

Experimentally, bond length dimerization due to Peierls distortions in CNTs can be studied by measuring its effect on the CNTs' vibrational spectrum using Raman scattering [136, 137]. The most intense Raman lines in the CNT spectrum correspond to totally symmetric vibrations in the Brillouin zone center. Among these vibrations the radial breathing mode is of particular interest, because its frequency uniquely depends on the CNT diameter. It has been theoretically shown [138] that in armchair CNTs the radial and tangential motions for quinoid type dimerization are mixed, while the radial breathing mode and transverse mode for Kekule type dimerization are splitted.

It has been suggested [139] that structural instability of one-dimensional systems can be used as the physical basis for the operation of molecular electronic devices. For example, the mechanical deformation of CNTs can significantly change their electronic properties. In [140], the atomic and band structure of the single-walled carbon zigzag type nanotube (6, 0) as a function of its axial relative elongation ε (figure 7) has been calculated using the method of molecular orbitals in the tight binding approximation. It was shown that the ground state of the nanotube has a Kekule structure, however at a relative elongation $\varepsilon_t \approx 9\%$ a structural phase transition

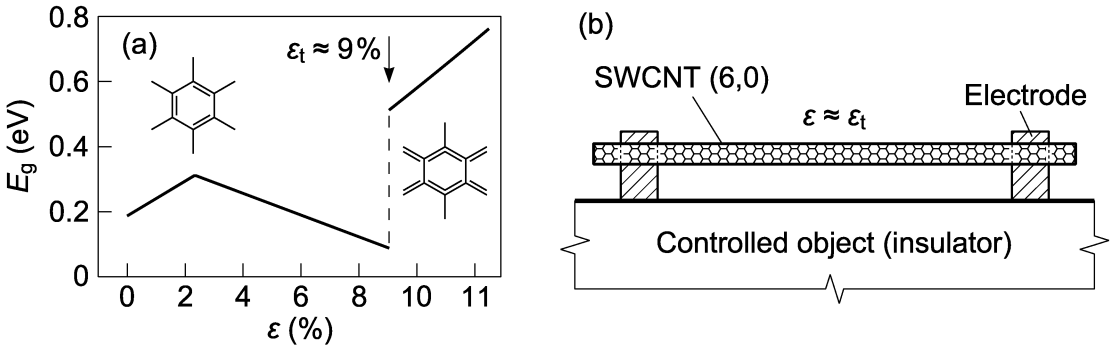

Figure 7. (a) The phase transition from Kekule to quinoid structure under tension (relative elongation ε) of the zigzag (6, 0) single-walled carbon nanotube and the scheme of a strain sensor (b) based on a prestrained nanotube; adapted from [140]. E_g is the band gap of the nanotube.

occurs that leads to the quinoid structure. Correspondingly, the nanotube switches from being a narrow bandgap to being a moderate bandgap semiconductor. This phenomenon can be used in a mechanical deformation sensor (figure 7). Band gap tuning by means of external strain is also possible for quasi-one-dimensional armchair graphene nanoribbons [141].

Beyond band structure calculations, the analysis of electrodynamic processes, both in single CNTs and in regular or irregular CNT ensembles, is an area of active research [142]. The properties of surface electronic waves (plasmons) in CNTs have been modeled using a hydrodynamic description of the charge carrier motion [143, 144]. However, such models prohibit relaxation processes that must be accounted for in the optical regime where resonant transitions are important. A better description of surface waves in CNTs is therefore provided by kinematic theory that accounts for attenuation [145]. Using this approach it has been shown, for instance, that a dispersionless propagation regime for surface waves in single CNTs is possible in the infrared regime, where the CNT effectively acts as an electronic waveguide.

Thermal radiation in systems with surface plasmons is influenced by near-field effects and is considerably different from blackbody radiation [146, 147]. Standing surface waves excited due to the strong reflection from CNT tips qualitatively distinguish CNTs from planar plasmonic structures, resulting in a distinct thermal radiation spectrum. CNTs can emit coherent thermal radiation in the terahertz range [148], acting as thermal nanoantennae [149].

The properties of CNTs can be modified in technologically useful ways by placing atoms or molecules within the nanotube [150]. Particularly, CNTs with opened ends can be filled using the capillary effect. Surface tension of the filling materials should be $\leqslant 0.2$ N/m [151]. This condition is satisfied for K, Rb, and Cs melts. Early research on filled CNTs was inspired by the idea of creating metal nanowires encapsulated within the CNT [152]. Within this paradigm, the CNT acts as a template for self-assembly of such nanowires [153, 154] and its structure becomes a sheath that protects the metal nanowire from damage by chemicals in its environment [155].

It should be kept in mind that there is interplay between the electronic properties of the CNT and the metal that fills it. For instance, if a SWCNT is filled with potassium atoms (figure 8(a)), the nanotube acts as an acceptor, capturing electrons from the dopant. In the band structure of SWCNTs encapsulating potassium, the nearly free electron state (that is located 3–4 eV above the Fermi level in pristine SWCNTs) is considerably affected by hybridization with the state of the encapsulated potassium [156, 157]. A theoretical analysis [158] of a SWCNT that captures one electron from the potassium atoms per 10 carbon atoms assumed the positive charge to be distributed within the volume of the nanotube and the negative—on its surface (figure 8(a)). The dependence of the Fermi quasimomentum of conduction electrons inside the nanotube on their concentration and on the tube radius was calculated in the single-electron approximation for an arbitrary number of sub-bands of the transverse motion. The stepwise dependence of the DC conduction G of the nanotube metallic subsystem on its radius was then calculated (figure 8(b)), and subsequently found partial experimental support [159]. This stepwise conductance of the doped nanotubes can be used in the design of nanoscale logic elements for computers [2].

Filling the cavity within an SWCNT offers great flexibility for tailoring its electronic properties, because SWCNTs can accommodate a wide variety of substances [160, 161]. Beyond metal wires, a particularly popular class of filled nanotubes are *carbon peapods*: systems with one or more encapsulated fullerenes inside the CNT [162, 163]. Some fullerenes, particularly C_{60}, form within CNTs spontaneously during synthesis and are hard to remove using standard purification methods [160, 162, 163]. Carbon peapods based on a wide variety of nanotubes encapsulating many other (endo)fullerene types, have also been produced [100, 164–169]. These

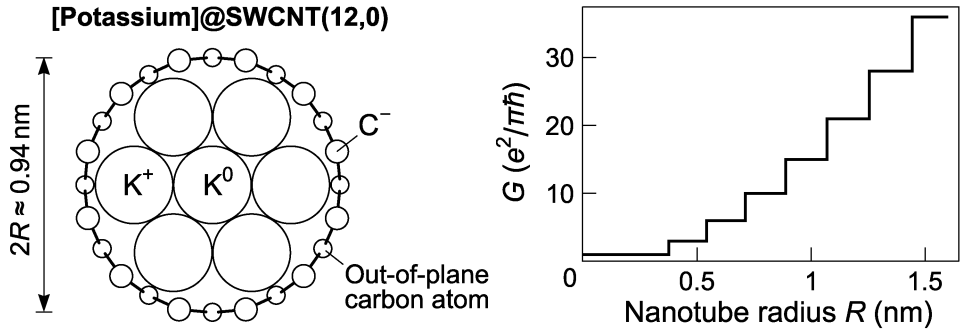

Figure 8. Left: cross-section of potassium filled zigzag (12, 0) single-walled carbon nanotube; K^0 and K^+ denote potassium neutral atom and positive ion with diameters of ≈0.3 nm; C^- denotes negatively charged carbon atom in the cross-section plane. (SWCNTs are acceptors of electrons: they capture one electron per ten carbon atoms.) Right: calculated electric DC conduction G (in units of $e^2/\pi\hbar \approx 77$ μS, where $\hbar = h/2\pi$ is the Planck constant) as a function of nanotube radius for electron density 14 nm^{-3} inside nanotube in the limit of zero absolute temperature ($T \to 0$); adapted from [158].

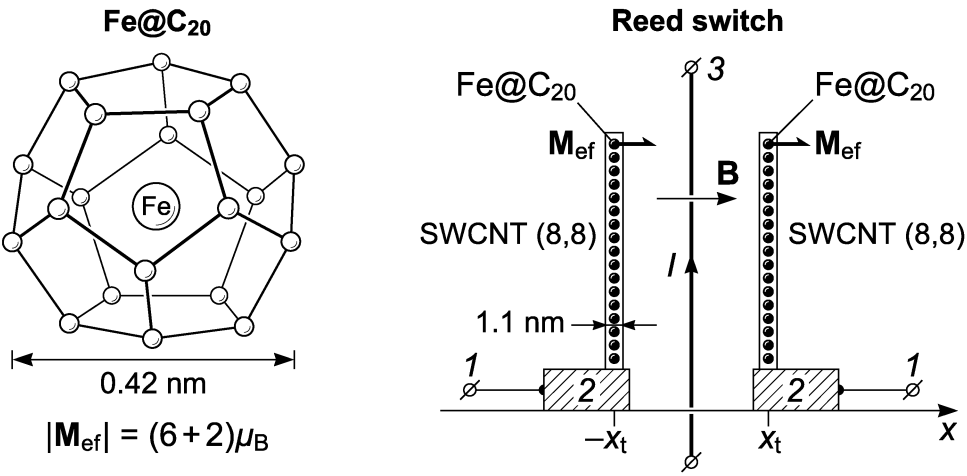

Figure 9. Left: a carbododecahedron with an iron atom inside Fe@C_{20} that has a spin magnetic moment $|\mathbf{M}_{ef}| = 8\mu_B$ (μ_B is the Bohr magneton). Right: scheme of a magnetic reed switch based on two armchair (8, 8) nanotubes filled with endofullerenes Fe@C_{20}: *1* is the controlled circuit, *2* is the electrode with the attached peapod nanotube, *3* is the wire with current I (placed below the nanotubes) used for inducing magnetic field with induction **B**; adapted from [164].

materials have properties that are distinct from those of both nanotubes and fullerenes, and are often considered a new class of self-assembled graphitic structures [170, 171]. They can also serve as chemical precursors for double-walled CNTs [172], another emerging class of materials that offers functionality beyond that of SWCNTs [173].

Diverse applications of carbon peapods in molecular optoelectronics and nanomechanics have been proposed, including single-electron transistors and charge-storage memory devices [174, 175], spin-qubit arrays for quantum computing [176, 177], nanoscale lasers [178], nanorelays and sensors [100, 164, 179].

An example of a carbon peapod-based device is a magnetic nanorelay: a reed switch based on two carbon nanotubes filled with magnetic endofullerenes (figure 9) [100, 164]. Applying a magnetic field leads to the bending of nanotubes, thereby closing the relay. The performance of nanorelays based on (8, 8) and (21, 21) single-walled nanotubes fully filled with Fe@C_{20} has been calculated. Turning on the nanorelay based on two (21, 21) nanotubes (diameter 2.85 nm) of 1 μm length with distance $2x_t \approx 31$ nm requires a magnetic field with induction $B \approx 30$ mT that can be produced by a direct current of $I = 150$ mA passing for a time interval exceeding 80 ns through the wire *3* (figure 9), positioned at a distance of 1 μm below the nanotubes.

Other configurations for nanotube-based devices controlled by magnetic fields are also possible. For instance, a force sensor can be based on the interaction between the ends of coaxial nanotubes, relating the direct current tunneling conductivity between the CNT ends to the measured force [179]. The operational characteristics of such a magnetic field sensor were estimated based on the magnetic force acting on coaxial (11, 11) nanotubes filled with magnetic endofullerenes $(Ho_3N)@C_{80}$ that have a magnetic moment of $21\mu_B$ [180]. The device

could potentially measure local magnetic fields with an excellent spatial resolution and a response time of approximately 0.3 ps.

Apart from filling the cavity of CNTs with guest materials, another popular strategy for tuning their properties is chemical functionalization of their sidewalls [181–184] or of their ends [185–187]. As produced, CNTs are typically bound into intertwined bundles with very low solubility in either water or organic solvents. Functionalization with solubilizing groups provides a major technological advantage in processing CNT-based materials. Selective and reversible functionalization also allows separating metallic and semiconducting CNTs [181]. Furthermore, functionalization can be used to promote self-assembly [186] or enable directed assembly of CNTs [187], to achieve biocompatibility [188], or to alter the optical and electronic properties of CNTs [189, 190].

CNT functionalization can either involve the formation of covalent bonds or exploit non-covalent interactions. The electronic parameters of CNTs can be reversibly tuned by very low concentrations of adsorbed gases, converting apparently semiconducting CNTs into apparent metals [191]. This finding suggests that CNTs can be used as sensitive chemical gas sensors. Chemical adsorption of H and F atoms on the open ends of an SWCNT can be used to control the movement of nanoelectromechanical devices [192, 193]. This modification gives the nanotube an electric dipole moment that can be set in motion by applying a nonuniform electric field.

In nanoelectronics, quantum wires such as CNTs are often embedded into a host matrix that affects their properties [194, 195]. In particular, the direct current (DC) electrical resistivity of a semiconductor quantum wire depends on interactions of electrons delocalized along the wire with longitudinal acoustic (LA) phonons in an insulating solid-state host matrix [196]. Currently, a nanocomputer with a bit logic based on arrays of nanowire lattices where each lattice site is a programmable transistor is being developed [197].

The environment can also affect electron transport in quasi-one-dimensional conductors in other ways. For instance, it has been shown that for a conductive carbyne chain or a carbon nanotube located in a dielectric environment with distributed inductance, an inductive soliton (or *inducton*) solution exists for the wavefunction of a single conductive electron [198]. The extent to which the current pulse of an inducton is compressed in the direction of motion increases with an increase in the inductance of the environment. An inductive environment could be realized, e.g., by placing a carbon nanotube on the surface of a thin insulating layer on top of a ferromagnetic material [199]. (The concept of an electrostatic inducton as an electron moving in a two-dimensional semiconductor quantum well parallel to the metal plane situated nearby has also been proposed [200].)

The DC electrical conductivity of 'epoxy resin + multi-walled nanotubes' composites is higher than for 'epoxy resin + single-walled nanotubes' composites with the same weight content of CNTs in a wide temperature range, 1.8–300 K [201, 202]. This difference is associated with a smaller number of contact barriers to electron transitions between individual multi-walled nanotubes. It was shown that the DC electrical conductivity of carbon nanotube arrays at cryogenic temperatures increases under electromagnetic irradiation (in the frequency range 0.5–7.3 THz) due to bolometric heating and changes in the rate of hopping migration of electrons under irradiation [202]. The kinetic inductance of individual nanotubes contributes to the low-frequency impedance of fibers composed of SWCNTs (at cryogenic temperatures and a constant electric bias) [203].

4. Two-dimensional systems

Graphene, a one atomic monolayer thick two-dimensional carbon crystal (figure 10), has garnered much attention in recent years [23, 204, 205]. It can be viewed as a relatively stable flat macromolecule with unique mechanical, electrical, optical, and chemical properties [206–210]. Although theoretically studied for decades [211–214], graphene had been assumed not to exist in free-standing form due to instability with respect to the formation of curved structures such as soot, fullerenes and nanotubes [215]. Because the properties of multi-layered graphene rapidly approach those of bulk graphite as the number of atomic monolayers, n, increases to about ten [216], there had been little hope of studying truly two-dimensional carbon structures experimentally. However, graphene monolayers have been obtained by mechanical exfoliation from bulk graphite and could be distinguished from double and few-layer ($n = 3$–10) structures, as well as from thin graphite slices by their optical properties [23, 215]. It has since been found that graphene exfoliation could be made more efficient if performed in certain solvents [217], mapping one possible route to industrial-scale production.

Alternative scalable approaches that enable producing large-area single- and few-monolayer graphene samples are thermal growth [218] and chemical vapour deposition [219–222]. Large-area CVD-grown graphene samples can be transferred onto appropriate substrates for device fabrication using polymer layers deposited on top of the graphene for mechanical support [223–225]. However, polymer residues left behind due to incomplete removal of the support layer are the dominant source of extrinsic doping reported in devices made

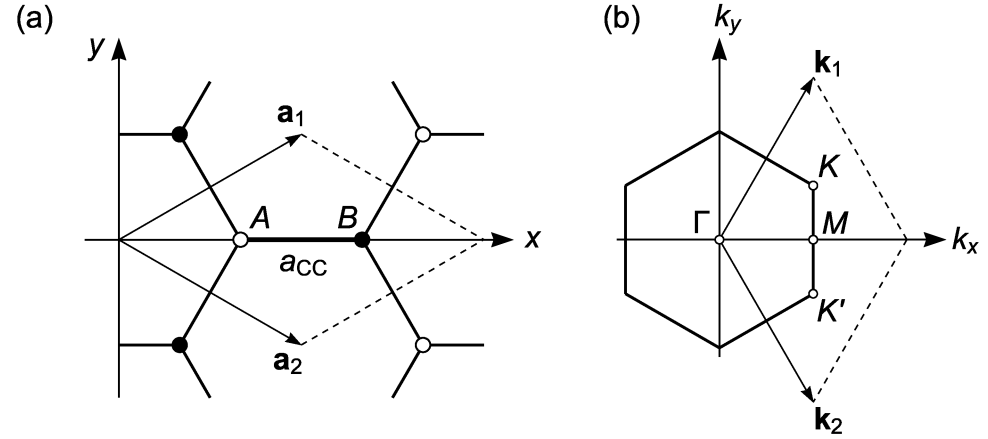

Figure 10. Structure of a single layer of graphene in real space (a) and in reciprocal space (b). The rhombic elementary unit cell with area $S_a = \sqrt{3}\,a^2/2$ is denoted by dotted lines in xy plane (a), where $a = a_{CC}\sqrt{3} = 0.246$ nm is the length of vectors $\mathbf{a}_1$ and $\mathbf{a}_2$. The hexagon in $k_x k_y$ plane (b) is the boundary of the first Brillouin zone with area $S_k = (2\pi)^2/S_a = (8/\sqrt{3})(\pi/a)^2$. Here $\mathbf{a}_1$ and $\mathbf{a}_2$ are the translational vectors, $\mathbf{k}_1$ and $\mathbf{k}_2$ are vectors reciprocal to $\mathbf{a}_1$ and $\mathbf{a}_2$. The length of reciprocal vectors $\mathbf{k}_1$ and $\mathbf{k}_2$ is $4\pi/\sqrt{3}\,a$. Nonequivalent graphene lattice sites are denoted by *A* and *B*. The distance between Γ and *M* points is $2\pi/\sqrt{3}\,a$.

from CVD-grown graphene [226]. Such contamination can be avoided by using an inorganic buffer layer, such as CVD-grown hexagonal boron nitride, between the graphene film and the supporting polymer layer [227]. Furthermore, bottom-up organic synthesis of narrow straight-edged stripes of graphene, known as nanoribbons, has recently become possible with atomic precision [14, 15, 228].

The availability of graphene stimulated extensive interdisciplinary research spanning physics, chemistry, and biology, and the development of a variety of technological applications. A combination of extraordinary electronic and mechanical characteristics makes graphene particularly suitable for applications in nanoelectromechanical devices.

Graphene is the strongest material ever tested, with an intrinsic tensile strength of 130 GPa and a Young's modulus of 1 TPa [229]. The spring constant of suspended graphene sheets measured using atomic force microscopes is of the order of 1 N/m [230]. Sheets can be bent to very large angles (exceeding 54°) with little strain and preserve excellent conductive properties in this conformation [231].

The band theory of graphite was first developed by P R Wallace [211]. The conduction and valence bands of graphene are formed by the non-hybridized p_z orbitals of sp^2 carbon atoms and in simplest tight-binding approximation have the dispersion relation [232, 233]

$$E(k_x, k_y) = \pm\gamma_0\sqrt{1 + 4\cos^2\frac{k_y a}{2} + 4\cos\frac{k_y a}{2}\cos\frac{\sqrt{3}\,k_x a}{2}},$$

where $\gamma_0 = 2.8$ eV is the nearest-neighbor hopping energy and $a = 0.246$ nm is the lattice constant; the plus sign corresponds to the conduction and the minus sign to the valence band (see figure 11). Because each carbon atom contributes a single π electron, the valence band is fully occupied by electrons and the conduction band is vacant. The sp^2 hybridized states (σ-states) form occupied and empty bands with a wide band gap (≈6.3 eV at Γ point) [234, 235]. From the dispersion relation it then follows that an infinite graphene sheet is a zero-bandgap semiconductor, with the valence and conduction bands touching at the corners of the first Brillouin zone (Dirac points *K* and *K′* in figure 10). Two of the six Dirac points are independent, the rest are equivalent by symmetry [214, 236]. The tight-binding approximation predicts zero band gap for graphene nanoribbons with a zigzag edge, whereas the band gap for nanoribbons with an armchair edge is either zero or finite depending on their width [237].

Electrons in the graphene lattice have a zero effective mass and are described by a 2D analogue of the Dirac equation [232, 238]. The material displays high charge carrier mobilities, above 15,000 $cm^2/(V\,s)$ [215]. The temperature dependence of the mobility is weak between 10 and 100 K, implying that scattering by defects is dominant at these temperatures [239, 240]. The intrinsic limit on the charge carrier mobility at room temperature imposed by scattering on graphene's acoustic phonons is about 200,000 $cm^2/(V\,s)$ at a carrier density of 10^{12} cm^{-2} [240, 241]. This corresponds to a conductivity of 10^8 S, the highest of any material. There is recent experimental evidence of superconductivity in graphene [242, 243].

Optoelectronic properties of graphene, including the charge carrier mobility, are sensitive to the presence of a substrate, of contaminants or defects, and to the topology of the graphene sample. The atomic thickness of graphene limits its interaction with electromagnetic fields. Consequently, there is considerable interest in hybrid

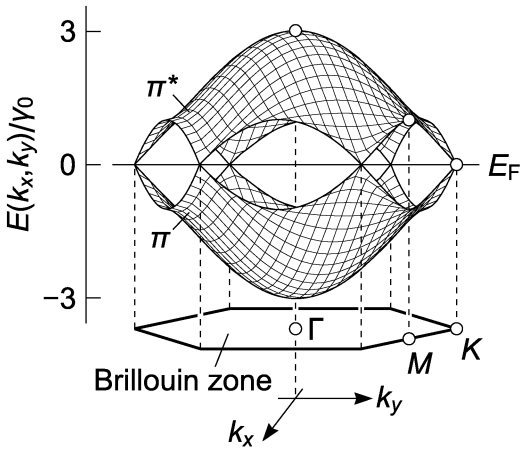

Figure 11. Band structure of π electrons in the first Brillouin zone of virgin graphene calculated in the tight-binding approximation (see formula in the text); π and π^* denote bonding and antibonding states, respectively; E_F is the Fermi level.

composites of graphene and optically active nanomaterials, such as semiconductor quantum dots, nanowires, and metallic nanoparticles that increase the light–matter interaction and extend the functionality of graphene-based optoelectronic devices [244, 245]. It has been theoretically and experimentally demonstrated that microwave absorptance of graphene can be enhanced considerably by depositing graphene sheets on a dielectric substrate and tuned by the choice of the dielectric permittivity and the thickness of the substrate [246]. Propagation of an electron beam over a graphene/dielectric sandwich structure induces an electromagnetic wave with a frequency tuned by varying the graphene doping, the number of graphene sheets, or the distance between sheets [247]. This effect could be used to develop coherent terahertz radiation sources with a tunable frequency. Near-field coupling between charge carriers in graphene and surface plasmon excitations in metal nanoparticles can be used to control the surface plasmon resonance of metallic nanostructures [248–250]. Metallic nanoparticles can also serve as antennas for concentrating light into nanoscopic volumes to enhance photoabsorption in the graphene layer [251]. Transfer of charge carriers, including hot charge carriers, between graphene and metal nanoparticles, and vice versa, has also been observed [244].

Electronic devices are constructed from fragments of the infinite graphene sheet whose properties may be largely determined by the crystallographic orientation of their edges [252]. Systems that are commonly studied in this context are graphene nanoribbons (GNRs), defined as strips of graphene less than 50 nm wide for which edge effects are significant [237]. Such structures can be produced by a variety of techniques, including exfoliation of strips from nanoscale blocks of graphite [253, 254], by 'unzipping' of CNTs [255, 256], or by atomically precise bottom-up synthesis [257, 258].

GNRs with both armchair and zigzag-shaped edges have been theoretically and experimentally shown to have band gaps [259, 260]. For GNRs with armchair shaped edges band gaps arise from both quantum confinement and edge effects, and for GNRs with zigzag shaped edges they are a consequence of a staggered sublattice potential on the hexagonal lattice due to edge magnetization [259, 260]. For instance, molecular orbital calculations of the electronic energy band structure for zigzag type graphene nanoribbons consisting of *n* zigzag atomic chains (*n*zGNR) show that a narrow nanoribbon (4zGNR) is a semiconductor in both the antiferromagnetic and the ferromagnetic states (figure 12) [261]. However, a wide nanoribbon (10zGNR) in the antiferromagnetic state is a semiconductor (band gap ≈0.1 eV), while in the ferromagnetic state it is a half-metal: an electrical conductor for one spin orientation (figure 13).

For some applications, the form factor of GNRs provides an attractive alternative to related materials, such as CNTs. For instance, field emission of electrons from GNRs can be used to create an alternating current electric generator [262]. In contrast to known schemes where field emission occurs from the butt end of a nanowire (a bunch of CNTs) [263], GNRs allow for a more simple and production-friendly construction in the form of a double-clamped graphene nanoribbon cathode placed above the flat anode surface [262].

Conformational changes and defects can affect both mechanical and electronic properties of graphene. For instance, although the elastic modulus of the material is preserved even at high concentrations of sp^3-type defects, the presence of vacancy defects leads to a significant deterioration of its mechanical properties [264]. Because of high defect concentrations, in nanoribbons produced from lithographically patterned exfoliated graphene the mean free path of charge carriers between scattering events is on the order of ten nanometers [260, 265], whereas ballistic electron transport on a length scale greater than ten micrometers has been observed in nanoribbons epitaxially grown on silicon carbide [266, 267].

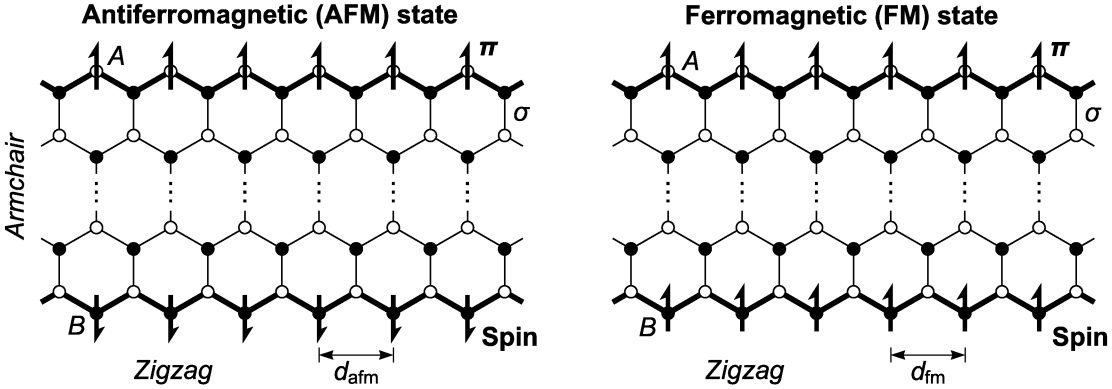

Figure 12. Antiferromagnetic and ferromagnetic states of zigzag nanoribbons are determined by the spin orientation of π electrons in edge chains formed by *A*- (light) and *B*-site (dark) carbon atoms; d_{afm} and d_{fm} are the translational periods for zigzag nanoribbon in antiferromagnetic and ferromagnetic states, respectively. At the edges of nanoribbons σ bonds of carbon atoms are passivated by hydrogen atoms.

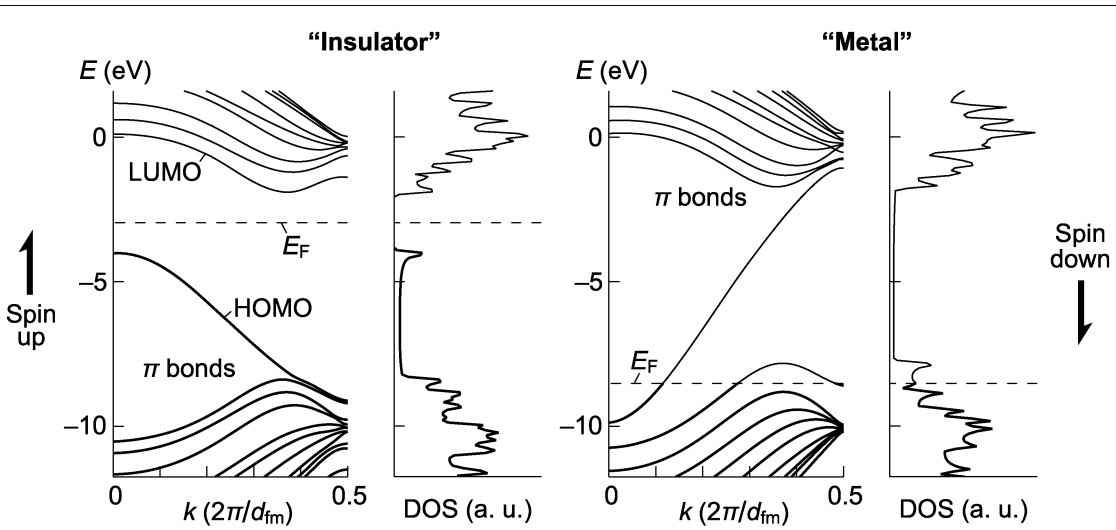

Figure 13. Half-metal band structure (dependence of single π-electron energy E on wavenumber k along nanoribbon) and density of states (DOS) for 10zGNR in the ferromagnetic state calculated using UHF PM3. Here E_F is the Fermi level, HOMO (LUMO) is the highest occupied (lowest unoccupied) molecular orbital, and $d_{fm} = 0.247$ nm is the translational period. Band gap for insulating spin orientation is ≈2.1 eV.

Topological defects, such as disclinations (heptagons or pentagons) and dislocations (heptagon–pentagon dipoles) are also essential to engineering wrinkled graphene structures with tailored mechanical and physical properties [268–271]. Such novel carbon structures are of great interest for electronic and nanoelectromechanical devices, and theoretical methods for describing their properties need to be developed. Both continuum approaches that allow predicting the three-dimensional configuration of such structures and stress fields in them and atomistic approaches are currently explored [270].

Conceptually, deformed graphene structures bridge the gap between purely two-dimensional graphene monolayers and closed carbon surfaces such as fullerenes and CNTs, as well as purely three-dimensional structures, such as turbostratic graphite and pores in diamond. Although the stability of some theoretically proposed carbon allotropes has been disputed [272], many such structures have been observed experimentally for decades. Among them are nanocones that can be viewed as graphene sheets rolled into conical surfaces with closed apeces and open bases. Nanocones can form naturally in the carbon plasma and have long been studied both experimentally [273] and theoretically [274–276]. To form a cone with strain-free, seamless wrapping a sector with an angle $n\pi/3$, where n is an integer between 1 and 5, must be cut from a graphene sheet. Therefore, the cone angle can only assume discrete values $\alpha = 2\arcsin(1 - n/6)$, and n pentagonal disclinations are needed to form a curved cone tip [277]. Deviations from these cone angles can occur due to the presence of linear defects and have been observed, e.g., in cones that naturally occur on the surface of graphite aggregates embedded in calcites [278]. The subclass of nanocones with five pentagonal disclinations, corresponding to the

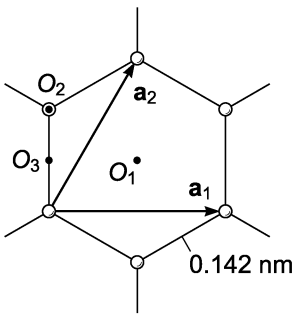

(a)

Funnel apex	Angle of rotation
O_1, center of regular hexagon	$\pi/3$, $2\pi/3$, π, $4\pi/3$, $5\pi/3$
O_2, vertex of regular hexagon	$2\pi/3$, $4\pi/3$
O_3, center of edge of regular hexagon	π

(b)

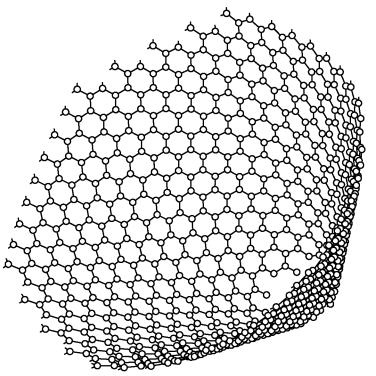

(c)

Figure 14. (a) Fragment of the graphene lattice (with points of the type O_1, O_2 and O_3), $\mathbf{a}_1$, $\mathbf{a}_2$ are the basis vectors (see also figure 10(a)). (b) Rotations around points O_1, O_2 or O_3, are possible in the graphene group symmetry (within the accuracy of a shift by the vectors $\mathbf{a}_1$ and $\mathbf{a}_2$). (c) Monolayer carbon funnel determined by the rotation with the center at the O_1 point by the angle π.

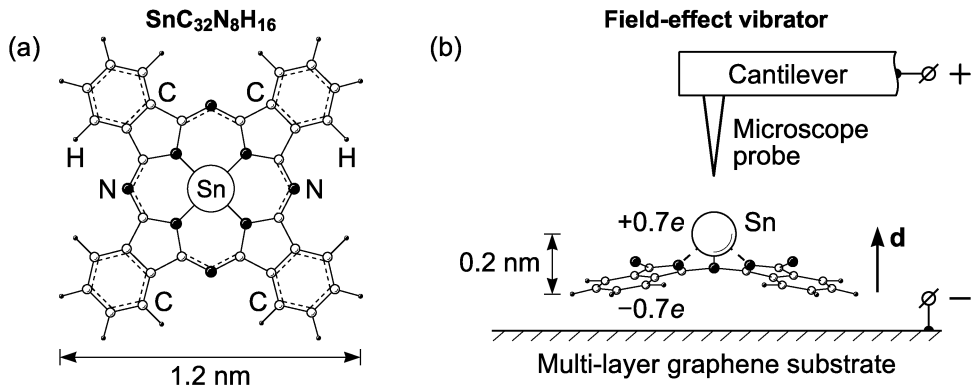

Figure 15. (a) Top view of funnel-like carbon-based molecule $SnC_{32}N_8H_{16}$ (i.e. SnPc). (b) Scheme of an electromechanical vibrator based on a single SnPc molecule placed over multi-layer graphene substrate (as electrode) under a microscope probe (side view). The vibrator is operated by applying an electric field between the probe and the substrate; e is the elementary charge, $\mathbf{d}$ is the intrinsic electric dipole moment of the molecule.

smallest possible cone angle of 19.2°, are called nanohorns [279]. Nanocones and nanohorns have been proposed for diverse applications ranging from drug delivery [280] to use as catalytic supports [281] and protective caps for scanning tunneling microscope tips [282].

Related carbon allotropes that have not yet been observed experimentally are funnels with an open apex [283]. Whereas factorization of the hexagonal lattice by a shift to the chiral vector $\mathbf{C}(n, m) = n\mathbf{a}_1 + m\mathbf{a}_2$ gives the (n, m) nanotube [284], factorization by a rotation from the symmetry group of the lattice gives a conical surface—a funnel. These structures should not be confused with hypothetical hybrid 1D/2D carbon superarchitectures built from seamlessly joined graphene sheets with apertures and carbon nanotubes that may also be referred to as 'carbon nanofunnels' and have been proposed as components of nanoscale sieves [285]. To classify monolayer funnels it is sufficient to consider the conjugacy classes of the group of rotations and their action on the lattice [75]. Only 8 funnel types defined by rotations around apexes O_1, O_2, and O_3 are possible (figure 14). Graphene funnels could serve as concentrators of solar radiation in nonimaging optics [286] or find applications in nanolithography [287]. Carbon funnels could also be functionalized with donors (e.g., hydrogen atoms) at one edge and with acceptors (e.g., boron atoms) at the other edge. Such functionalization would give a funnel an intrinsic dipole moment, enabling its use as an electrically controlled actuator (see, e.g., [288]). This approach can be used for constructing graphene-based electronic and nanoelectromechanical devices, such as cantilevers [289] that are promising for applications in chemical and biological sensors [290].

Single-molecule devices based on funnel-shaped organic molecules with a dipole moment, such as SnPc (where Pc denotes the macrocyclic ring $C_{32}H_{16}N_8$, figure 15(a)), have already been envisaged. These devices include a single-photon source [6] and an electromechanical generator [291]. In SnPc, electric charge from the central metal atom transfers to the macrocyclic ring [292], creating a nonzero electric dipole moment perpendicular to the macrocycle plane [293]. A change in the dipole moment when the macromolecule is turned

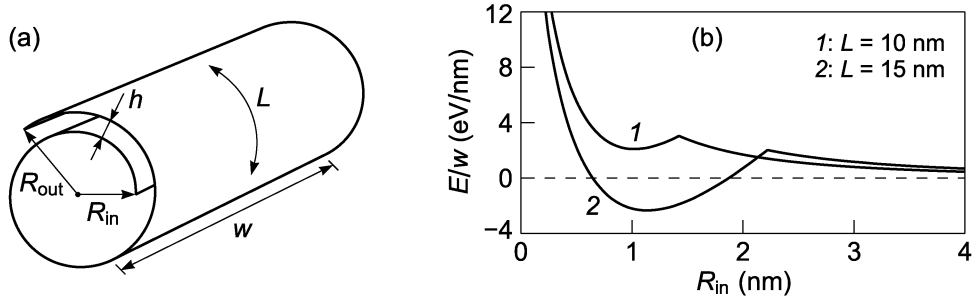

Figure 16. (a) Model of carbon nanoscroll (CNS) considered as an Archimedean spiral determined by inner radius R_{in} and outer radius R_{out} with interlayer distance $h = d_g = 0.335$ nm rolled from graphene sheet of width w and length L. (b) Calculated potential energy per width of carbon single-layer nanoscrolls E/w as a function of the inner radius R_{in} for nanoscrolls rolled from graphene nanoribbons with the length $L = 10$ nm and 15 nm. Minima in curves at $R_{in} \approx 1$ nm correspond to the stable states of the nanoscrolls.

inside out [294, 295] may lead to the emission of a photon. The energy barrier for turning an adsorbed SnPc molecule inside out is about 2.5 eV [296, 297]. A terahertz electromechanical vibrator based on a single SnPc molecule is analogous to vibrators based on a carbon nanotube bunch [263] or a double clamped graphene nanoribbon [262] that use the electron field emission effect. In this device, the SnPc molecule (a source of field-emitted electrons) could be placed on a multi-layer graphene substrate under a microscope probe (figure 15(b)).

Another class of structures closely related to graphene are carbon nanoscrolls (CNSs): defect-free 2D graphene sheets rolled into 1D spirals (figure 16(a)). Such structures can be manufactured by rolling up monolayer graphene on an inorganic substrate in solution [298]. High-quality CNSs have also recently be obtained using polymer-assisted liquid exfoliation [299]. Some properties of these materials, such as high charge carrier mobility, are similar to those of graphene and CNTs, whereas others are determined by their unique topology that allows π–π interactions between parts of the graphene sheet that form different layers of the CNS [300, 301]. The electronic structure of CNSs is determined by chirality, with higher densities of states at the Fermi level for metallic CNSs as compared to metallic SWCNTs and smaller energy gaps for semiconducting CNSs as compared to semiconducting SWCNTs [300, 301]. Because of their intercalated structure, CNSs have been proposed for applications in hydrogen storage [302, 303], supercapacitors [304–306], and batteries [304, 307]. Because the diameter of CNSs can be controlled by charge injection or intercalation, they can also be used in nanomechanical devices.

Understanding the stability and the dynamics of rolling and unrolling graphene sheets is essential to the development of CNS technology. The standard computational technique for such studies is atomistic molecular dynamics [304, 308, 309]; coarse-grained approaches have also been employed [310]. For modeling the operational characteristics of CNS-based nanoelectromechanical devices, atomistic modeling is of limited utility, and macroscopic semianalytical and numerical modeling of the structural and energetic characteristics of CNSs must be used [311]. This approach allows determining the geometrical dimensions of graphene nanoribbons that can form stable and energetically favorable CNSs, calculating the barriers for rolling graphene nanoribbons into CNSs and for unrolling CNSs into nanoribbons, as well as the CNS lifetime, as a function of the nanoribbon dimensions. At room temperature, nanoscrolls with a layer overlap length of about 1nm are found to be stable [311]; see also figure 16(b). It was calculated [312] that a square lattice of graphene/boron nitride nanoscrolls positioned perpendicularly to the carbon nanotubes forms a new metamaterial with negative refractive index (for light from near infrared to yellow).

The extremely high mobility of charge carriers in graphene-based materials predestined the popularity of these materials in electronics, particularly for high-frequency devices [313–315]. Graphene field-effect transistors can have operating frequencies in the teraherz range [316], and complete electronic circuits based on graphene devices monolithically integrated into a silicon carbide wafer with operating frequencies ~10 GHz have been manufactured [315]. Because graphene-based materials are flexible, biocompatible, and their electronic properties are sensitive to deformation and the adsorption of foreign molecules, these materials are popular in chemical and biological sensing applications [317–319]. A unique combination of electronic and mechanical properties makes graphene particularly attractive for nanoelectromechanical applications, e.g., nanodynamometers [320, 321]. In such devices, the mobile upper layer is in mechanical and electrical contact with two stationary lower graphene layers placed on two gold electrodes. An external force acting on the top layers of bilayer graphene can cause a relative shift δx of this layer, leading to a change in the electrical conductivity (registered by ammeter) between the layers. The interaction force between layers returns the top layer of graphene to its initial position after removal of the external force (see, review on Van der Waals, Casimir, and Lifshitz forces in [322]).

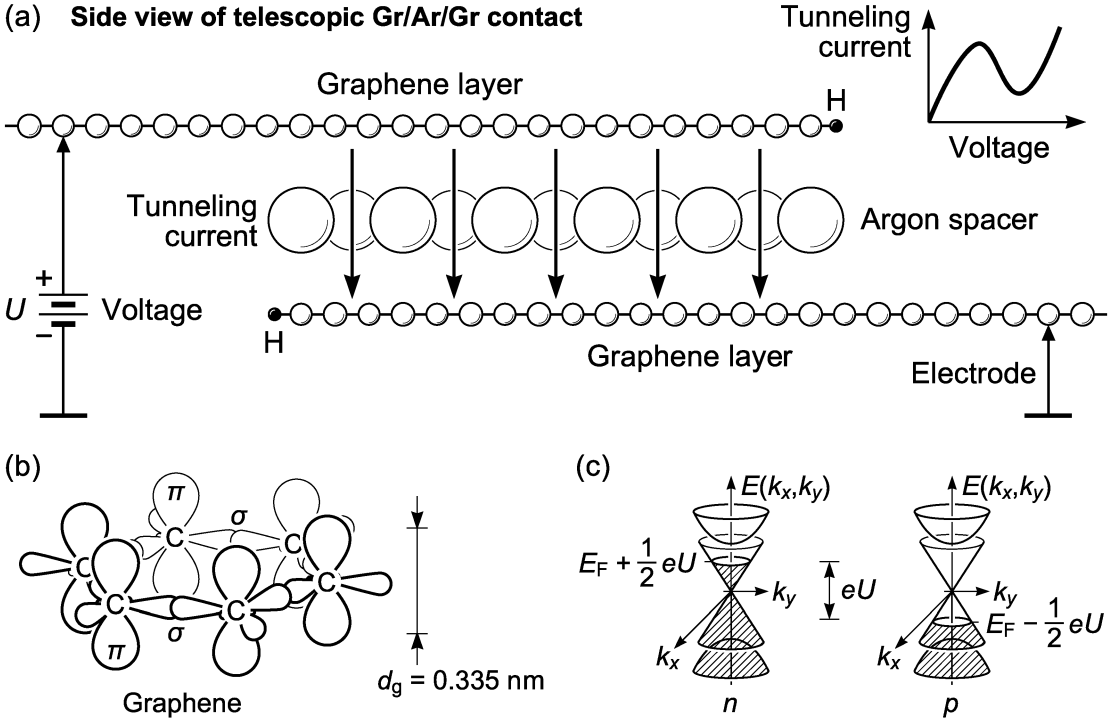

Figure 17. (a) Telescopic electrical contact between graphene layers (passivated at the edges by hydrogen atoms) with a dielectric argon spacer showing the negative differential resistance for tunneling current through the contact; adapted from [323]. (b) Fragment of graphene layer; d_g is the thickness of the graphene layer equal to the distance between atomic planes in graphite. (c) Band scheme $E(k_x, k_y)$ for π electrons in the vicinity of K points of Brillouin zone of graphene layers with positive (p) and negative (n) electric potential $\pm U/2$; states occupied by electrons are hatched.

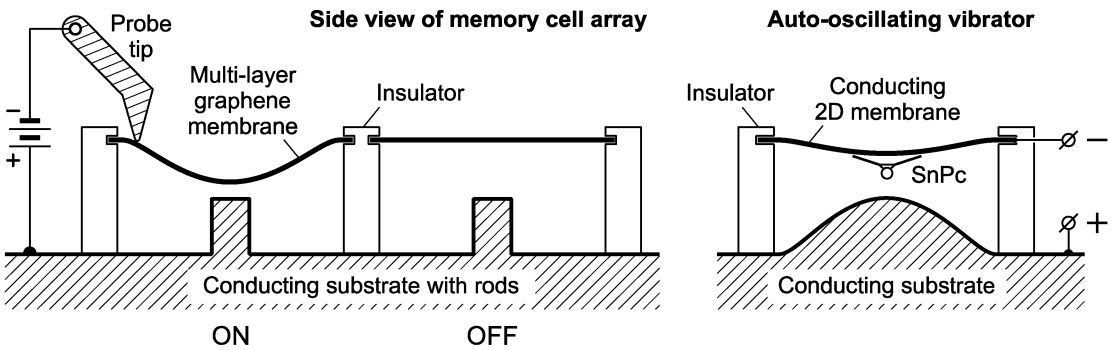

Figure 18. Left: scheme of the nonvolatile memory cell based on bending of conducting multi-layer graphene membrane circularly clamped in insulating barrier and positioned over conducting rod covered by graphene or graphite in ON state (left) and OFF state (right); the probe tip is used for switching between the OFF and ON states or reading the memory cell state. Memory cell can operate by applying a voltage of about 1 V for a membrane with diameter >250 nm, thickness of 3.4 nm (10 graphene layers), distance between the membrane and the rod <2 nm and rod diameter of 50 nm. The cell can be erased by applying the electric potential of the same polarity; adapted from [332]. Right: envisaged scheme of auto-oscillating system based on conducting 2D membrane and SnPc funnel-shaped molecule positioned over conducting substrate. The vibrator is operated by applying stationary electric field.

A new type of graphene-based nanoelectronic device is a telescopic electrical contact between two flat graphene layers with a dielectric (e.g., argon) spacer that functions as a tunneling diode (figure 17) [323]. A negative differential resistance (similar to a semiconductor tunnel diode [324]) is found for such a device. This behavior may originate from the interference of electronic wavefunctions in the bilayer region [325, 326] and/or a change of filling of c-band subbands of one graphene layer by electrons and v-band subbands of the other graphene layer by holes when an electrical bias is applied. The capacitance of the contact between the graphene layers with the argon spacer has been calculated (taking into account the quantum contribution [327, 328]).

Graphene-based nanoelectromechanical systems can be used as memory cells, with a variety of device architectures implemented or considered (see, e.g., figure 18). Switching between the conducting ON and non-conducting OFF states of the memory cell commonly occurs as a result of a controlled relative displacement of graphene layers [329, 330]. However, the possibility of relative sliding of the layers [331] limits the lifetime of the

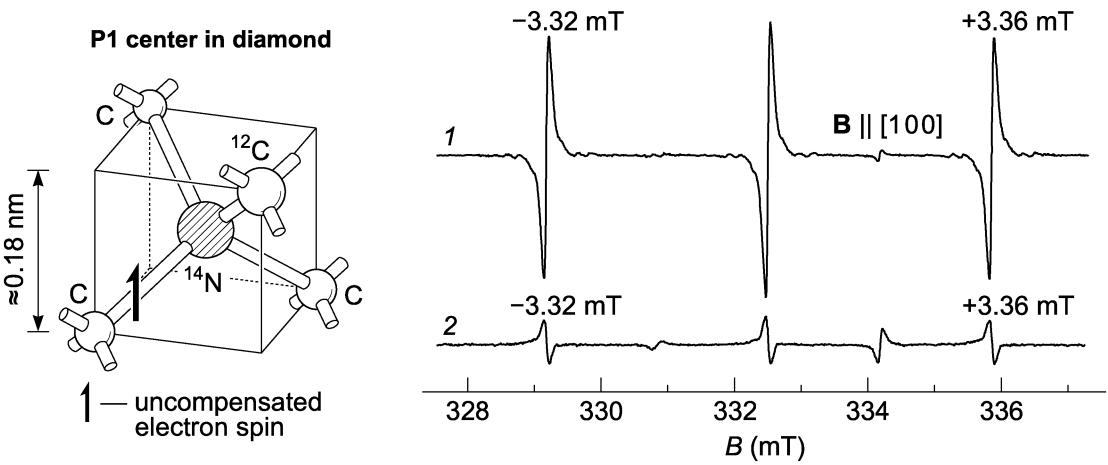

Figure 19. Left: nitrogen in *C* form (referred to as a 'P1 center' in ESR spectroscopy) substituting carbon atom in diamond crystal matrix. Right: in-phase CW ESR spectra of P1 centers in a high-temperature high pressure treated synthetic diamond single crystal, measured at room temperature in the dark for two levels of microwave power supplied to the H_{102} resonator: (*1*) 70 μW and (*2*) 70 mW. The magnetic induction vector **B** is perpendicular to the (1 0 0) plane; the shifts of the low-field (−) and high-field (+) satellites relative to the central component are indicated; the amplification for shown signals are the same; adapted from [353].

ON and OFF states before spontaneous switching occurs. Nanoelectromechanical memory cells where switching between the conducting ON and non-conducting OFF states occurs by bending a graphene membrane under an applied electrostatic force could ensure much longer lifetimes of the ON and OFF states, making such cells suitable for long-term information archiving (figure 18) [332]. The principles underlying the operation of the memory cell (figure 18) and the molecular vibrator based on SnPc funnel-shaped molecule (figure 15) can be used for construction of an auto-oscillating system of a new type. (Elements of engineering of such solutions are discussed in [333, 334].)

5. Zero-dimensional (point) defects in diamond matrix

A unique combination of physico-chemical properties makes diamonds attractive both for fundamental research and for technological applications [335]. The extraordinary thermal conductivity of diamonds in conjunction with their wide band gap and low electron affinity makes them promising for applications in high-power and high-temperature optoelectronic devices [336, 337]. Neutron irradiation leads to formation of sp^2 bonded regions [338, 339] and nanosized pores [340] in sp^3 diamond matrix. The migration energies for various types of defects in diamond are considerably higher than for defects in silicon [341]. Therefore, diamond is an excellent matrix for the formation of stable devices based on defects and disordered regions. Diamonds could find applications in quantum computing: qubit prototypes have been built from nitrogen atom + carbon vacancy complexes in the diamond crystal lattice [342–344]. Synthetic diamonds that are heavily doped with boron can be used to study superconductivity at and above liquid helium temperature [345, 346] and can be used as electrodes for detection of neurochemicals in the human brain at room temperature [347].

Nitrogen is the most common impurity in diamond and gives crystals a distinctive yellowish tint [348]. In optical spectroscopy electrically neutral nitrogen atom substitution in the diamond lattice is referred to as nitrogen in *C* form (figure 19). Its concentration can be deduced from infrared absorption spectra, where it is responsible for a sharp peak at 1344 cm^{-1} and a broader feature at 1130 cm^{-1} [349]. This impurity is typical of synthetic diamond single crystals produced under high-pressure and high-temperature [350], as well as of polycrystalline CVD diamond grown in a hydrocarbon/nitrogen atmosphere that facilitates doping [351, 352].

Continuous wave electron spin resonance (CW ESR) spectroscopy is a powerful non-destructive technique that provides a microwave 'look' through a magnetic 'window' on the point defects and dislocations with uncompensated electron spin in crystalline matrices [354, 355]. Due to an uncompensated electron spin, nitrogen in *C* form is easily detectable by CW ESR spectroscopy, where it is referred to as a 'P1 center'. The P1 center is a deep electron donor (ionization energy ≈1.7 eV) [356]. Four valence electrons of the nitrogen atom form N–C bonds, and the fifth extra valence electron (uncompensated electron spin) is localized on any one of the four N–C bonds (closer to the carbon atom) [357]. The signature of this impurity in CW ESR spectra is shown in figure 19; satellites '±' of the central line are caused by the interaction of an uncompensated electronic spin with the nuclear magnetic moment of the ^{14}N atom [353]; scan rate 1 mT/min; microwave frequency 9.321 GHz; magnetic field modulation frequency 100 kHz; modulation amplitude 0.02 mT (for details of ESR

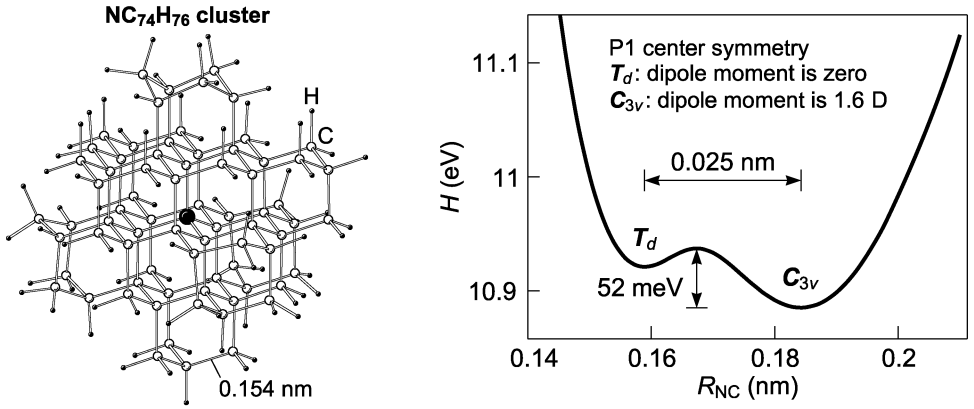

Figure 20. Left: P1 center simulated by NC_{74} cluster passivated by 76 hydrogen atoms; N atom indicated as a dark ball in the center of the cluster. Right: heat of formation H for $NC_{74}H_{76}$ cluster versus N–C bond length R_{NC} between N atom and the nearest C atom in [1 1 1] direction; adapted from [363]. The point symmetry groups T_d and C_{3v} of P1 center are shown. (Thermal energy at room temperature is approximately equal 26 meV. Electric dipole moment $|\mathbf{d}| = 1$ D corresponds to $0.393ea_0$, where e is the elementary charge, a_0 is the Bohr radius.)

technique for carbon materials see also [358]). Increasing microwave electromagnetic radiation power leads to an inversion of the signal from nitrogen atoms in synthetic diamond monocrystals [359, 360] and polycrystalline diamond films [361] at room temperature. This inversion of the in-phase CW ESR signal is associated with the bistability of the nitrogen atom (figure 19) coordination in diamond matrix. This phenomenon may be used to monitor the structural perfection of diamonds, as the improvement of structural perfection leads to a decrease of the microwave power at which the CW ESR signal is inverted. Noninverted satellites at ± 1.67 mT from the central component (figure 19) are caused by *A* centers (pairs of exchange-coupled nitrogen atoms in the neighbor sites of diamond lattice). Aggregation of nitrogen atoms in crystalline diamond can be controlled using thermal annealing at 1800 °C in a hydrogen atmosphere [362].

The stationary states of nitrogen in *C* form (P1 center) have been calculated [363] using the method of molecular orbitals (figure 20). A design of a maser that could operate at room temperature based on the interaction of P1 center with microwaves and phonons has been proposed [361]. A room-temperature maser based on the action of microwaves in conjunction with green laser illumination was implemented [364] on N–*V* centers (nitrogen + vacancy of carbon atom) in diamond.

Diamonds with point defects of the crystal structure are promising for nanophotonic device applications [365]. For instance, injection lasers can be developed using radiative transitions of electrons and/or holes on single defects that have zero-phonon lines in the photoluminescence spectrum [366]. In a diamond *p*–*i*–*n*-diode, the emission of single photons has been observed from single electrically neutral N–*V* centers in the *i*-region for a direct bias at room temperature [367].

6. Outlook

Carbon-based low-dimensional systems and point defects in diamond have great potential for applications in next-generation electronics, photonics, acoustics, and spintronics. However, realizing this potential requires perfecting methods for the production, diagnostics, and theoretical analysis of such materials.

The electromagnetic, optical, acoustic, and thermal properties of three-dimensional crystals with length scales greater than 100 nm are described by band theory [368, 369]. The physical properties of solitary atoms, molecules, and atomic clusters with dimensions smaller than a few nanometers can be calculated using *ab initio* quantum chemical methods. However, neither approach works adequately at length scales between about 1 and 100 nm. The utility of band theory for such low-dimensional systems is limited due to violation of translational symmetry [370]. On the other hand, the computational cost of *ab initio* calculations quickly becomes prohibitively high as size increases. Atomic and molecular theory also does not analyze how translational symmetry determines the structure and properties of matter, viewing them as emergent directly from the electronic structure of constituent atoms [371].

The rational design of low-dimensional carbon-based structures for applications in devices with length scales of 0.1 μm to 1 nm requires a quantum theory of states and processes in such systems. This theory should describe states and processes in the building blocks of the system (individual atoms, molecules, or clusters), as well as account for the consequences of agglomeration of these blocks into low-dimensional structures.

Today, the most promising research directions in the field of carbon-based nanostructured material science and engineering include (see [372] and also [373–377]):

(1) Development of a quantum theory of ionization equilibrium and of hopping charge transfer in low-dimensional systems for hydrogen and solar energetics. This advance will facilitate the creation of new graphene-like materials for photovoltaic cells and of stable ('non-poisoned') electrodes for water photolysis.

(2) Further integration of magnetism into semiconductor micro- and nanoelectronics. Development of novel approaches to engineering of magnetic carbon low-dimensional systems on silicon wafers will allow extending their applications in spintronics.

(3) Development of methods for the formation of low-dimensional systems (such as fibers, scrolls, and ribbons) for nanoscale device elements based on the interaction of compression plasma fluxes and intense laser radiation with the surface of synthetic diamond crystals.

(4) Establishment of the relation between the mechanical strength of diamond and silicon carbide crystals and the Fermi level position in the electron energy band diagram of the crystals. It is determined by the intrinsic defects of crystal structure and the presence of impurity atoms with varying electrical and magnetic activity. The solution to this problem is critical for simulating the degradation of these materials in power electronics and optics.

Future research on carbon-based nanostructures must emphasize exploring the interrelation between their electronic, magnetic, optical, thermal, chemical, and mechanical properties. It is important to keep in mind that modification of one material property (e.g., optimization of mechanical strength) often affects other properties (e.g., electrical conductivity). Novel nanoscale devices, including many of those described in this paper, are frequently enabled by a synergy of these diverse material properties. The vast landscape of carbon allotropes and carbon-based nanomaterials allows finding combinations of material properties that are needed for a very wide range of applications. This approach opens the door both to nanoscale analogues of existing devices and to fundamentally new technology.

Acknowledgments

The work is supported by the Belarusian National Research Program 'Convergence-2020', by the Belarusian Republican Foundation for Fundamental Research (grant No. F18R-253), by the EU Framework Programme for Research and Innovation Horizon 2020 (grant No. H2020-MSCA-RISE-2015-690968 NANOGUARD2AR), and by the Vietnam National Foundation for Science and Technology Development (NAFOSTED) under grant number 103.01-2017.309.

ORCID iDs

N A Poklonski https://orcid.org/0000-0002-0799-6950
N N Hieu https://orcid.org/0000-0001-5721-960X

References

[1] Roco M C, Mirkin C A and Hersam M C 2011 *Nanotechnology Research Directions for Societal Needs in 2020: Retrospective and Outlook* (Dordrecht: Springer)
[2] Waser R (ed) 2012 *Nanoelectronics and Information Technology: Advanced Electronic Materials and Novel Devices* (Weinheim: Wiley)
[3] Borisenko V E and Ossicini S 2012 *What is What in the Nanoworld: A Handbook on Nanoscience and Nanotechnology* (Weinheim: Wiley)
[4] Sladkova T A (ed) 2007 *Carbon Investigation–Progress and Problems* (Moscow: Nauka) [in Russian]
[5] Hirsch A 2010 *Nat. Mater.* **9** 868–71
[6] Poklonski N A 2010 Low-dimensional carbon systems *Proc. of Int. Winter School on Semiconductor Physics 2010, St.-Petersburg–Zelenogorsk, 25 Feb.–1 March 2010* (St.-Petersburg: Ioffe Physical-Technical Institute) pp 48–52 [in Russian]
[7] Konov V I 2012 *Laser Photonics Rev.* **6** 739–66
[8] Makarov G N 2013 *Phys. Usp.* **56** 643–82
[9] Khomich V Y and Shmakov V A 2015 *Phys. Usp.* **58** 455–65
[10] Baklanov M R, de Marneffe J F, Shamiryan D, Urbanowicz A M, Shi H, Rakhimova T V, Huang H and Ho P S 2013 *J. Appl. Phys.* **113** 041101
[11] Gurovich B A, Dolgii D I, Kuleshova E A, Velikhov E P, Ol'shanskii E D, Domantovskii A G, Aronzon B A and Meilikhov E Z 2001 *Phys. Usp.* **44** 95–105
[12] Skowron S T, Lebedeva I V, Popov A M and Bichoutskaia E 2013 *Nanoscale* **5** 6677–92
[13] Bejan A and Lorente S 2013 *J. Appl. Phys.* **113** 151301

[14] Cai J *et al* 2010 *Nature* **466** 470–3
[15] Mehdi Pour M *et al* 2017 *Nat. Commun.* **8** 820
[16] Dresselhaus M S 2014 *Mater. Res. Lett.* **2** 1–9
[17] Peierls R 1991 *Sov. Phys. Usp.* **34** 817
[18] Kroto H W, Heath J R, O'Brien S C, Curl R F and Smalley R E 1985 *Nature* **318** 162–3
[19] Ekimov A I and Onushchenko A A 1981 *JETP Lett.* **34** 345–9 http://www.jetpletters.ac.ru/ps/1517/article_23187.shtml
[20] Kudryavtsev Y P 1999 The discovery of carbyne *Carbyne and Carbynoid Structures* ed R B Heimann, S E Evsyukov and L Kavan (Dordrecht: Kluwer) pp 1–6
[21] Iijima S 1991 *Nature* **354** 56–8
[22] Ertchak D P, Efimov V G and Stelmakh V F 1997 *J. Appl. Spectrosc.* **64** 433–60
[23] Novoselov K S, Geim A K, Morozov S V, Jiang D, Zhang Y, Dubonos S V, Grigorieva I V and Firsov A A 2004 *Science* **306** 666–9
[24] Gazalé M J 1999 *Gnomon: From Pharaohs to Fractals* (Princeton: Princeton University Press)
[25] Tsu R 2011 *Superlattice to Nanoelectronics* (Amsterdam: Elsevier)
[26] Shur M 1987 *GaAs Devices and Circuits* (New York: Springer)
[27] Volkov A F and Kogan S M 1969 *Sov. Phys. Usp.* **11** 881–903
[28] Pepper D M, Feinberg J and Kukhtarev N V 1990 *Sci. Am.* **263** 62–74
[29] Gaponenko S V and Demir H V 2018 *Applied Nanophotonics* (Cambridge: Cambridge University Press)
[30] Brazhkin V V 2009 *Phys. Usp.* **52** 369–76
[31] Inagaki M and Radovic L R 2002 *Carbon* **40** 2279–82
[32] Heimann R B, Evsvukov S E and Koga Y 1997 *Carbon* **35** 1654–8
[33] Pogrebnjak A D, Ponomarev A G, Shpak A P and Kunitskii Y A 2012 *Phys. Usp.* **55** 270–300
[34] Andrievski R A 2013 *Phys. Usp.* **56** 261–8
[35] Elias D C *et al* 2009 *Science* **323** 610–3
[36] Churilov G N 2000 *Instrum. Exp. Tech.* **43** 1–10
[37] Makarova T L 2001 *Semiconductors* **35** 243–78
[38] Fowler P W and Manolopoulos D E 1995 *An Atlas of Fullerenes* (Oxford: Clarendon)
[39] Mroz P, Tegos G P, Gali H, Wharton T, Sarna T and Hamblin M R 2007 *Photochem. Photobiol. Sci.* **6** 1139–49
[40] Abrahamse H and Hamblin M R 2016 *Biochem. J.* **473** 347–64
[41] Gao F, Zhao G L, Yang S and Spivey J J 2013 *J. Am. Chem. Soc.* **135** 3315–8
[42] Vidal S, Marco-Martínez J, Filippone S and Martín N 2017 *Chem. Commun.* **53** 4842–4
[43] Heeger A J 2014 *Adv. Mater.* **26** 10–28
[44] Liu Y, Zhao J, Li Z, Mu C, Ma W, Hu H, Jiang K, Lin H, Ade H and Yan H 2014 *Nat. Commun.* **5** 5293
[45] Whaley K B, Kocherzhenko A A and Nitzan A 2014 *J. Phys. Chem.* C **118** 27235–44
[46] Pillai S, Ravensbergen J, Antoniuk-Pablant A, Sherman B D, van Grondelle R, Frese R N, Moore T A, Gust D, Moore A L and Kennis J T M 2013 *Phys. Chem. Chem. Phys.* **15** 4775–84
[47] Lee D, Forsuelo M A, Kocherzhenko A A and Whaley K B 2017 *J. Phys. Chem.* C **121** 13043–51
[48] Shakhov F M and Kidalov S V 2014 *Phys. Solid State* **56** 1622–5
[49] Curl R F 1993 *Phil. Trans. R. Soc. Lond.* A **343** 19–32
[50] Lozovik Y E and Popov A M 1997 *Phys. Usp.* **40** 717–37
[51] Heath J R 1992 Synthesis of C_{60} from small carbon clusters: A model based on experiment and theory *Fullerenes: Synthesis, Properties, and Chemistry of Large Carbon Clusters* (*ACS Symposium Series* vol 481) ed G S Hammond and V J Kuck (Washington, DC, USA: ACS) ch 1, pp 1–23
[52] Prinzbach H, Weiler A, Landenberger P, Wahl F, Wörth J, Scott L T, Gelmont M, Olevano D and von Issendorff B 2000 *Nature* **407** 60–3
[53] Poklonski N A, Ratkevich S V and Vyrko S A 2015 *J. Phys. Chem.* A **119** 9133–9
[54] Léonard C, Carter S and Handy N C 2003 *Chem. Phys. Lett.* **370** 360–5
[55] Berry R S and Smirnov B M 2013 *Phys. Usp.* **56** 973–98
[56] Shirkov D V 2009 *Phys. Usp.* **52** 549–57
[57] Perrin M L *et al* 2014 *Nat. Nanotechnol.* **9** 830–4
[58] Poklonskii N A, Kislyakov E F, Bubel' O N and Vyrko S A 2002 *J. Appl. Spectrosc.* **69** 323–7
[59] Poklonski N A, Kislyakov E F, Bubel' O N and Vyrko S A 2004 *Proc. SPIE* **5509** 179–86
[60] Jones R O 1999 *J. Chem. Phys.* **110** 5189–200
[61] Killblane C, Gao Y, Shao N and Zeng X C 2009 *J. Phys. Chem.* A **113** 8839–44
[62] Portmann S, Galbraith J M, Schaefer H F, Scuseria G E and Lüthi H P 1999 *Chem. Phys. Lett.* **301** 98–104
[63] Barnard A S, Russo S P and Snook I K 2003 *J. Chem. Phys.* **118** 5094–7
[64] Jiang Q and Chen Z P 2006 *Carbon* **44** 79–83
[65] Chelikowsky J R 1992 *Phys. Rev.* B **45** 12062–70
[66] Yamaguchi Y and Maruyama S 1998 *Chem. Phys. Lett.* **286** 336–42
[67] Irle S, Zheng G, Elstner M and Morokuma K 2003 *Nano Lett.* **3** 1657–64
[68] Qian H J, Wang Y and Morokuma K 2017 *Carbon* **114** 635–41
[69] Irle S, Zheng G, Elstner M and Morokuma K 2003 *Nano Lett.* **3** 465–70
[70] Lebedeva I V, Knizhnik A A, Popov A M and Potapkin B V 2012 *J. Phys. Chem.* C **116** 6572–84
[71] Lee G D, Wang C Z, Yu J, Yoon E and Ho K M 2003 *Phys. Rev. Lett.* **91** 265701
[72] Sinitsa A S, Lebedeva I V, Popov A M and Knizhnik A A 2017 *J. Phys. Chem.* C **121** 13396–404
[73] Bubel' O N, Vyrko S A, Kislyakov E F and Poklonskii N A 2000 *JETP Lett.* **71** 508–10
[74] Horoyski P J, Thewalt M L W and Anthony T R 1996 *Phys. Rev.* B **54** 920–9
[75] Poklonski N A, Vlassov A T and Vyrko S A 2011 *Finite Symmetry Groups. Fundamentals and Applications* (Minsk: P. Brouka Belarusian Encyclopedia) [in Russian]
[76] Tanigaki K, Ebbesen T W, Saito S, Mizuki J, Tsai J S, Kubo Y and Kuroshima S 1991 *Nature* **352** 222–3
[77] Lunin R, Velikodny Y, Bulychev B and Kulbachinskii V 2015 *Polyhedron* **102** 664–7
[78] Fan W and Zhang R Q 2009 *Front. Phys. China* **4** 315–26
[79] Lau C S, Sadeghi H, Rogers G, Sangtarash S, Dallas P, Porfyrakis K, Warner J, Lambert C J, Briggs G A D and Mol J A 2016 *Nano Lett.* **16** 170–6

[80] Gobbi M, Bedoya-Pinto A, Golmar F, Llopis R, Casanova F and Hueso L E 2012 *Appl. Phys. Lett.* **101** 102404
[81] Kocherzhenko A A, Siebbeles L D A and Grozema F C 2011 *J. Phys. Chem. Lett.* **2** 1753–6
[82] Aviram A and Ratner M A 1974 *Chem. Phys. Lett.* **29** 277–83
[83] Roth S *et al* 1998 *Synth. Met.* **94** 105–10
[84] Metzger R M 2003 *Chem. Rev.* **103** 3803–34
[85] Perrin M L, Galan E, Eelkema R, Grozema F, Thijssen J M and van der Zant H S J 2015 *J. Phys. Chem.* C **119** 5697–702
[86] Perrin M L, Burzurí E and van der Zant H S J 2015 *Chem. Soc. Rev.* **44** 902–19
[87] Jia C *et al* 2018 *Sci. Adv.* **4** eaat8237
[88] Park H, Park J, Lim A K L, Anderson E H, Alivisatos A P and McEuen P L 2000 *Nature* **407** 57–60
[89] Winkelmann C B, Roch N, Wernsdorfer W, Bouchiat V and Balestro F 2009 *Nat. Phys.* **5** 876–9
[90] Pasupathy A N *et al* 2005 *Nano Lett.* **5** 203–7
[91] Park H, Lim A K L, Alivisatos A P, Park J and McEuen P L 1999 *Appl. Phys. Lett.* **75** 301–3
[92] Khadem Hosseini V, Ahmadi M T, Afrang S and Ismail R 2017 *J. Electron. Mater.* **46** 4294–8
[93] Leuenberger M N and Loss D 2001 *Nature* **410** 789–93
[94] Grose J E, Tam E S, Timm C, Scheloske M, Ulgut B, Parks J J, Abruña H D, Harneit W and Ralph D C 2008 *Nat. Mater.* **7** 884–9
[95] Kasumov A Y *et al* 2005 *Phys. Rev.* B **72** 033414
[96] Brown R M, Ito Y, Warner J H, Ardavan A, Shinohara H, Briggs G A D and Morton J J L 2010 *Phys. Rev.* B **82** 033410
[97] Zheng H, Zhao X, Wang W W, Dang J S and Nagase S 2013 *J. Phys. Chem.* C **117** 25195–204
[98] Shinohara H and Tagmatarchis N 2015 *Endohedral Metallofullerenes: Fullerenes with Metal Inside* (Chichester, UK: Wiley)
[99] Wu B, Wang T, Feng Y, Zhang Z, Jiang L and Wang C 2015 *Nat. Commun.* **6** 6468
[100] Poklonski N A, Kislyakov E F, Vyrko S A, Hieu N N, Bubel' O N, Siahlo A I, Lebedeva I V, Knizhnik A A, Popov A M and Lozovik Y E 2010 *J. Nanophotonics* **4** 041675
[101] Hughes T V and Chambers C R 1889 Manufacture of carbon filaments *U.S. Patent* 405,480
[102] Radushkevich L V and Lukyanovich V M 1952 *Sov. J. Phys. Chem.* **26** 88–95 [in Russian]
[103] Monthioux M and Kuznetsov V L 2006 *Carbon* **44** 1621–3
[104] Eletskii A V 2010 *Phys. Usp.* **53** 863–92
[105] Kharlamova M V 2013 *Phys. Usp.* **56** 1047–73
[106] Lee S W and Campbell E E B 2013 *Curr. Appl. Phys.* **13** 1844–59
[107] Peng B, Locascio M, Zapol P, Li S, Mielke S L, Schatz G C and Espinosa H D 2008 *Nat. Nanotechnol.* **3** 626–31
[108] Wang X, Li Q, Xie J, Jin Z, Wang J, Li Y, Jiang K and Fan S 2009 *Nano Lett.* **9** 3137–41
[109] Pop E, Mann D, Wang Q, Goodson K and Dai H 2006 *Nano Lett.* **6** 96–100
[110] Laird E A, Kuemmeth F, Steele G A, Grove-Rasmussen K, Nygård J, Flensberg K and Kouwenhoven L P 2015 *Rev. Mod. Phys.* **87** 703–64
[111] Takesue I, Haruyama J, Kobayashi N, Chiashi S, Maruyama S, Sugai T and Shinohara H 2006 *Phys. Rev. Lett.* **96** 057001
[112] Lortz R *et al* 2009 *Proc. Natl. Acad. Sci. USA* **106** 7299–303
[113] Tibbetts G G 1984 *J. Cryst. Growth* **66** 632–8
[114] Bethune D S, Klang C H, de Vries M S, Gorman G, Savoy R, Vazquez J and Beyers R 1993 *Nature* **363** 605–7
[115] Tessonnier J P and Su D S 2011 *ChemSusChem* **4** 824–47
[116] Lu J and Miao J 2012 *Nanoscale. Res. Lett.* **7** 356
[117] Thess A *et al* 1996 *Science* **273** 483–7
[118] Lu W and Lieber C M 2006 *J. Phys. D: Appl. Phys.* **39** R387–406
[119] Dubrovskii V G, Cirlin G E and Ustinov V M 2009 *Semiconductors* **43** 1539–84
[120] Hamada N, Sawada S and Oshiyama A 1992 *Phys. Rev. Lett.* **68** 1579–81
[121] Saito R, Fujita M, Dresselhaus G and Dresselhaus M S 1992 *Appl. Phys. Lett.* **60** 2204–6
[122] Odom T W, Huang J L, Kim P and Lieber C M 2000 *J. Phys. Chem.* B **104** 2794–809
[123] Blase X, Benedict L X, Shirley E L and Louie S G 1994 *Phys. Rev. Lett.* **72** 1878–81
[124] Lu X and Chen Z 2005 *Chem. Rev.* **105** 3643–96
[125] Yang L, Anantram M P, Han J and Lu J P 1999 *Phys. Rev.* B **60** 13874–8
[126] Heyd R, Charlier A and McRae E 1997 *Phys. Rev.* B **55** 6820–4
[127] Reich S, Thomsen C and Maultzsch J 2004 *Carbon Nanotubes: Basic Concepts and Physical Properties* (Weinheim: Wiley)
[128] Poklonski N A, Kislyakov E F and Podenok S L 2003 Electronic structure of metallic single-wall carbon nanotubes: tight-binding versus free-electron approximation *Physics, Chemistry and Application of Nanostructures. Reviews and Short Notes to Nanomeeting-2003, Minsk, 20–23 May 2003* ed V E Borisenko, S V Gaponenko and V S Gurin (Singapore: World Scientific) pp 186–9
[129] Hieu N N and Hieu N V 2014 *Phys. Status Solidi* B **251** 1614–8
[130] Zhang Y and Han M 2011 *Physica* E **43** 1774–8
[131] Poklonski N A, Kislyakov E F, Kuzmin L, Tarasov M and Campbell E E B 2005 On the phonon mechanism of energy transfer from conduction electrons to lattice in single-wall metallic carbon nanotubes at low temperatures *Physics, Chemistry and Application of Nanostructures. Reviews and Short Notes to Nanomeeting-2005, Minsk, 24–27 May 2005* ed V E Borisenko, S V Gaponenko and V S Gurin (Singapore: World Scientific) pp 235–9
[132] Saito R, Dresselhaus G and Dresselhaus M S 1998 *Physical Properties of Carbon Nanotubes* (London: Imperial College Press)
[133] Poklonski N A, Kislyakov E F, Hieu N N, Bubel O N, Vyrko S A, Popov A M and Lozovik Y E 2008 *Chem. Phys. Lett.* **464** 187–91
[134] Tretiak S, Kilina S, Piryatinski A, Saxena A, Martin R L and Bishop A R 2007 *Nano Lett.* **7** 86–92
[135] Dumont G, Boulanger P, Côté M and Ernzerhof M 2010 *Phys. Rev.* B **82** 035419
[136] Dresselhaus M S, Dresselhaus G, Saito R and Jorio A 2005 *Phys. Rep.* **409** 47–99
[137] Oron-Carl M, Hennrich F, Kappes M M, von Löhneysen H and Krupke R 2005 *Nano Lett.* **5** 1761–7
[138] Poklonski N A, Kislyakov E F, Hieu N N, Vyrko S A, Bubel' O N and Viet N A 2010 *Comput. Mater. Sci.* **49** S231–4
[139] Krieger Y H 1999 *J. Struct. Chem.* **40** 594–619
[140] Poklonski N A, Ratkevich S V, Vyrko S A, Kislyakov E F, Bubel' O N, Popov A M, Lozovik Y E, Hieu N N and Viet N A 2012 *Chem. Phys. Lett.* **545** 71–7
[141] Nguyen C V, Hieu N V, Toan H N, Nhan L C, Anh N T and Hieu N N 2017 *J. Electron. Mater.* **46** 3815–9
[142] Maffucci A, Maksimenko S A, Miano G and Slepyan G Y 2017 Electrical conductivity of carbon nanotubes: Modeling and characterization *Carbon Nanotubes for Interconnects: Process, Design and Applications* ed A Todri-Sanial, J Dijon and A Maffucci (Basel: Springer) pp 101–28

[143] Jiang X 1996 *Phys. Rev.* B **54** 13487–90
[144] Yannouleas C, Bogachek E N and Landman U 1996 *Phys. Rev.* B **53** 10225–36
[145] Slepyan G Y, Maksimenko S A, Lakhtakia A, Yevtushenko O and Gusakov A V 1999 *Phys. Rev.* B **60** 17136–49
[146] Shchegrov A V, Joulain K, Carminati R and Greffet J J 2000 *Phys. Rev. Lett.* **85** 1548–51
[147] Henkel C, Joulain K, Carminati R and Greffet J J 2000 *Opt. Commun.* **186** 57–67
[148] Wang R, Xie L, Hameed S, Wang C and Ying Y 2018 *Carbon* **132** 42–58
[149] Nemilentsau A M, Slepyan G Y and Maksimenko S A 2007 *Phys. Rev. Lett.* **99** 147403
[150] Gately R D and in het Panhuis M 2015 *Beilstein J Nanotechnol.* **6** 508–16
[151] Cook J, Sloan J and Green M L H 1997 *Fullerene Sci. Technol.* **5** 695–704
[152] Iijima S and Ichihashi T 1993 *Nature* **363** 603–5
[153] Ye X R, Lin Y, Wang C and Wai C M 2003 *Adv. Mater.* **15** 316–9
[154] Elías A L *et al* 2005 *Nano Lett.* **5** 467–72
[155] Gao X P, Zhang Y, Chen X, Pan G L, Yan J, Wu F, Yuan H T and Song D Y 2004 *Carbon* **42** 47–52
[156] Miyamoto Y, Rubio A, Blase X, Cohen M L and Louie S G 1995 *Phys. Rev. Lett.* **74** 2993–6
[157] Miyake T and Saito S 2002 *Phys. Rev.* B **65** 165419
[158] Poklonskii N A, Kislyakov E F, Fedoruk G G and Vyrko S A 2000 *Phys. Solid State* **42** 1966–71
[159] Suzuki S, Maeda F, Watanabe Y and Ogino T 2003 *Phys. Rev.* B **67** 115418
[160] Kharlamova M V 2016 *Prog. Mater. Sci.* **77** 125–211
[161] Monthioux M, Flahaut E and Cleuziou J P 2006 *J. Mater. Res.* **21** 2774–93
[162] Smith B W, Monthioux M and Luzzi D E 1998 *Nature* **396** 323–4
[163] Smith B W, Monthioux M and Luzzi D E 1999 *Chem. Phys. Lett.* **315** 31–6
[164] Poklonski N A, Kislyakov E F, Vyrko S A, Hieu N N, Bubel' O N, Siahlo A I, Lebedeva I V, Knizhnik A A, Popov A M and Lozovik Y E 2010 A low-voltage magnetic nanorelay design *SPIE Newsroom* (https://doi.org/10.1117/2.1201010.003091)
[165] Zólyomi V *et al* 2014 *J. Phys. Chem.* C **118** 30260–8
[166] Sloan J *et al* 2000 *Chem. Phys. Lett.* **316** 191–8
[167] Kataura H, Maniwa Y, Kodama T, Kikuchi K, Hirahara K, Suenaga K, Iijima S, Suzuki S, Achiba Y and Krätschmer W 2001 *Synth. Met.* **121** 1195–6
[168] Hirahara K, Suenaga K, Bandow S, Kato H, Okazaki T, Shinohara H and Iijima S 2000 *Phys. Rev. Lett.* **85** 5384–7
[169] Bandow S, Takizawa M, Kato H, Okazaki T, Shinohara H and Iijima S 2001 *Chem. Phys. Lett.* **347** 23–8
[170] Rochefort A 2003 *Phys. Rev.* B **67** 115401
[171] Iijima S 2002 *Physica* B **323** 1–5
[172] Ding F, Xu Z, Yakobson B I, Young R J, Kinloch I A, Cui S, Deng L, Puech P and Monthioux M 2010 *Phys. Rev.* B **82** 041403
[173] Moore K E, Tune D D and Flavel B S 2015 *Adv. Mater.* **27** 3105–37
[174] Lee C H, Kang K T, Park K S, Kim M S, Kim H S, Kim H G, Fischer J E and Johnson A T 2003 *Jpn. J. Appl. Phys.* **42** 5392–4
[175] Shimada T *et al* 2005 *Jpn. J. Appl. Phys.* **44** 469–72
[176] Ge L, Montanari B, Jefferson J H, Pettifor D G, Harrison N M and Briggs G A D 2008 *Phys. Rev.* B **77** 235416
[177] Yang W L, Xu Z Y, Wei H, Feng M and Suter D 2010 *Phys. Rev.* A **81** 032303
[178] He S L and Shen J Q 2006 *Chin. Phys. Lett.* **23** 211–3
[179] Popov A M, Lebedeva I V, Knizhnik A A, Lozovik Y E, Poklonski N A, Siahlo A I, Vyrko S A and Ratkevich S V 2014 *Comput. Mater. Sci.* **92** 84–91
[180] Wolf M, Müller K H, Skourski Y, Eckert D, Georgi P, Krause M and Dunsch L 2005 *Angew. Chem. Int. Ed.* **44** 3306–9
[181] Strano M S, Dyke C A, Usrey M L, Barone P W, Allen M J, Shan H, Kittrell C, Hauge R H, Tour J M and Smalley R E 2003 *Science* **301** 1519–22
[182] Balasubramanian K and Burghard M 2005 *Small* **1** 180–92
[183] Buffa F, Hu H and Resasco D E 2005 *Macromolecules* **38** 8258–63
[184] Dyke C A and Tour J M 2003 *Nano Lett.* **3** 1215–8
[185] Burghard M 2005 *Small* **1** 1148–50
[186] Lee K M, Li L and Dai L 2005 *J. Am. Chem. Soc.* **127** 4122–3
[187] Penzo E, Palma M, Wang R, Cai H, Zheng M and Wind S J 2015 *Nano Lett.* **15** 6547–52
[188] Meng L, Fu C and Lu Q 2009 *Prog. Nat. Sci.* **19** 801–10
[189] Bekyarova E, Itkis M E, Cabrera N, Zhao B, Yu A, Gao J and Haddon R C 2005 *J. Am. Chem. Soc.* **127** 5990–5
[190] Um J E, Chung C H, Lee D C, Yoo P J and Kim W J 2014 *RSC Adv.* **4** 42930–5
[191] Collins P G, Bradley K, Ishigami M and Zettl A 2000 *Science* **287** 1801–4
[192] Ershova O V, Lozovik Y E, Popov A M, Bubel' O N, Poklonskii N A and Kislyakov E F 2007 *Phys. Solid State* **49** 2010–4
[193] Ershova O V, Lebedeva I V, Lozovik Y E, Popov A M, Knizhnik A A, Potapkin B V, Bubel O N, Kislyakov E F and Poklonskii N A 2010 *Phys. Rev.* B **81** 155453
[194] Blanchet G B, Subramoney S, Bailey R K, Jaycox G D and Nuckolls C 2004 *Appl. Phys. Lett.* **85** 828–30
[195] Bokobza L 2007 *Polymer* **48** 4907–20
[196] Poklonskii N A, Kislyakov E F and Vyrko S A 2003 *Semiconductors* **37** 710–2
[197] Yao J, Yan H, Das S, Klemic J F, Ellenbogen J C and Lieber C M 2014 *Proc. Natl. Acad. Sci. USA* **111** 2431–5
[198] Poklonski N A, Vlassov A T, Vyrko S A, Kislyakov E F, Ratkevich S V and Siahlo A I 2013 Inducton: soliton-like motion of one electron in one-dimensional wire with inductance of environment *Physics, Chemistry and Applications of Nanostructures. Reviews and Short Notes: Proc. of Int. Conf. Nanomeeting-2013, Minsk, 28–31 May 2013* ed V E Borisenko *et al* (Singapore: World Scientific) pp 36–9
[199] Phan A D, Viet N A, Poklonski N A, Woods L M and Le C H 2012 *Phys. Rev.* B **86** 155419
[200] Bednarek S and Szafran B 2006 *Phys. Rev.* B **73** 155318
[201] Kuzhir P *et al* 2011 *Nanosci. Nanotechnol. Lett.* **3** 889–94
[202] Ksenevich V K *et al* 2008 *J. Appl. Phys.* **104** 073724
[203] Ksenevich V K, Gorbachuk N I, Poklonski N A, Samuilov V A, Kozlov M E and Wieck A D 2012 *Fullerenes, Nanotubes and Carbon Nanostructures* **20** 434–8
[204] Geim A K 2011 *Angew. Chem. Int. Ed.* **50** 6966–85
[205] Novoselov K S 2011 *Angew. Chem. Int. Ed.* **50** 6986–7002
[206] Eletskii A V, Iskandarova I M, Knizhnik A A and Krasikov D N 2011 *Phys. Usp.* **54** 227–58
[207] Galashev A E and Rakhmanova O R 2014 *Phys. Usp.* **57** 970–89

[208] Chernozatonskii L A, Sorokin P B and Artukh A A 2014 *Russ. Chem. Rev.* **83** 251–79
[209] Brownson D A C, Kampouris D K and Banks C E 2012 *Chem. Soc. Rev.* **41** 6944–76
[210] Antonova I V 2017 *Phys. Usp.* **60** 204–18
[211] Wallace P R 1947 *Phys. Rev.* **71** 622–34
[212] McClure J W 1956 *Phys. Rev.* **104** 666–71
[213] Slonczewski J C and Weiss P R 1958 *Phys. Rev.* **109** 272–9
[214] Semenoff G W 1984 *Phys. Rev. Lett.* **53** 2449–52
[215] Geim A K and Novoselov K S 2007 *Nat. Mater.* **6** 183–91
[216] Partoens B and Peeters F M 2006 *Phys. Rev.* B **74** 075404
[217] Yeon C, Yun S J, Lee K S and Lim J W 2015 *Carbon* **83** 136–43
[218] Tan H, Wang D and Guo Y 2018 *Coatings* **8** 40
[219] Malesevic A, Vitchev R, Schouteden K, Volodin A, Zhang L, Van Tendeloo G, Vanhulsel A and Van Haesendonck C 2008 *Nanotechnology* **19** 305604
[220] Reina A, Jia X, Ho J, Nezich D, Son H, Bulovic V, Dresselhaus M S and Kong J 2009 *Nano Lett.* **9** 30–5
[221] Li X *et al* 2010 *Nano Lett.* **10** 4328–34
[222] Liu W, Li H, Xu C, Khatami Y and Banerjee K 2011 *Carbon* **49** 4122–30
[223] Suk J W, Kitt A, Magnuson C W, Hao Y, Ahmed S, An J, Swan A K, Goldberg B B and Ruoff R S 2011 *ACS Nano* **5** 6916–24
[224] Song J, Kam F Y, Png R Q, Seah W L, Zhuo J M, Lim G K, Ho P K H and Chua L L 2013 *Nat. Nanotechnol.* **8** 356–62
[225] Kim H H, Chung Y, Lee E, Lee S K and Cho K 2014 *Adv. Mater.* **26** 3213–7
[226] Lin Y C, Lu C C, Yeh C H, Jin C, Suenaga K and Chiu P W 2012 *Nano Lett.* **12** 414–9
[227] Shautsova V, Gilbertson A M, Black N C G, Maier S A and Cohen L F 2016 *Sci. Rep.* **6** 30210
[228] Chen Y C, Cao T, Chen C, Pedramrazi Z, Haberer D, de Oteyza D G, Fischer F R, Louie S G and Crommie M F 2015 *Nat. Nanotechnol.* **10** 156–60
[229] Lee C, Wei X, Kysar J W and Hone J 2008 *Science* **321** 385–8
[230] Frank I W, Tanenbaum D M, van der Zande A M and McEuen P L 2007 *J. Vac Sci. Technol.* B **25** 2558–61
[231] Briggs B D, Nagabhirava B, Rao G, Geer R, Gao H, Xu Y and Yu B 2010 *Appl. Phys. Lett.* **97** 223102
[232] Castro Neto A H, Guinea F, Peres N M R, Novoselov K S and Geim A K 2009 *Rev. Mod. Phys.* **81** 109–62
[233] Jorio A, Saito R, Dresselhaus G and Dresselhaus M S 2011 *Raman Spectroscopy in Graphene Related Systems* (Weinheim: Wiley)
[234] Sheka E F, Popova N A and Popova V A 2018 *Phys. Usp.* **61** 645–91
[235] Katsnelson M I and Fasolino A 2017 Graphene: Basic properties *2D Materials: Properties and Devices* ed P Avouris, T F Heinz and T Low (Cambridge: Cambridge University Press) pp 5–256
[236] Katsnelson M I 2012 *Graphene: Carbon in Two Dimensions* (Cambridge: Cambridge University Press)
[237] Nakada K, Fujita M, Dresselhaus G and Dresselhaus M S 1996 *Phys. Rev.* B **54** 17954–61
[238] Gomes K K, Mar W, Ko W, Guinea F and Manoharan H C 2012 *Nature* **483** 306–10
[239] Morozov S V, Novoselov K S, Katsnelson M I, Schedin F, Elias D C, Jaszczak J A and Geim A K 2008 *Phys. Rev. Lett.* **100** 016602
[240] Chen J H, Jang C, Xiao S, Ishigami M and Fuhrer M S 2008 *Nat. Nanotechnol.* **3** 206–9
[241] Akturk A and Goldsman N 2008 *J. Appl. Phys.* **103** 053702
[242] Ludbrook B M *et al* 2015 *Proc. Natl. Acad. Sci. USA* **112** 11795–9
[243] Di Bernardo A *et al* 2017 *Nat. Commun.* **8** 14024
[244] Gilbertson A M *et al* 2015 *Nano Lett.* **15** 3458–64
[245] Koppens F H L, Mueller T, Avouris P, Ferrari A C, Vitiello M S and Polini M 2014 *Nat. Nanotechnol.* **9** 780–93
[246] Batrakov K, Kuzhir P, Maksimenko S, Volynets N, Voronovich S, Paddubskaya A, Valusis G, Kaplas T, Svirko Y and Lambin P 2016 *Appl. Phys. Lett.* **108** 123101
[247] Batrakov K and Maksimenko S 2017 *Phys. Rev.* B **95** 205408
[248] Yao Y, Kats M A, Genevet P, Yu N, Song Y, Kong J and Capasso F 2013 *Nano Lett.* **13** 1257–64
[249] Yao Y, Kats M A, Shankar R, Song Y, Kong J, Loncar M and Capasso F 2014 *Nano Lett.* **14** 214–9
[250] Zagorodko O, Spadavecchia J, Serrano A Y, Larroulet I, Pesquera A, Zurutuza A, Boukherroub R and Szunerits S 2014 *Anal. Chem.* **86** 11211–6
[251] Alonso-González P *et al* 2014 *Science* **344** 1369–73
[252] Ritter K A and Lyding J W 2009 *Nat. Mater.* **8** 235–42
[253] Li X, Wang X, Zhang L, Lee S and Dai H 2008 *Science* **319** 1229–32
[254] Mohanty N, Moore D, Xu Z, Sreeprasad T S, Nagaraja A, Rodriguez A A and Berry V 2012 *Nat. Commun.* **3** 844
[255] Kosynkin D V, Higginbotham A L, Sinitskii A, Lomeda J R, Dimiev A, Price B K and Tour J M 2009 *Nature* **458** 872–6
[256] Jiao L, Zhang L, Wang X, Diankov G and Dai H 2009 *Nature* **458** 877–80
[257] Talirz L, Ruffieux P and Fasel R 2016 *Adv. Mater.* **28** 6222–31
[258] Pachfule P, Shinde D, Majumder M and Xu Q 2016 *Nat. Chem.* **8** 718–24
[259] Son Y W, Cohen M L and Louie S G 2006 *Phys. Rev. Lett.* **97** 216803
[260] Han M Y, Özyilmaz B, Zhang Y and Kim P 2007 *Phys. Rev. Lett.* **98** 206805
[261] Poklonski N A, Kislyakov E F, Vyrko S A, Bubel' O N and Ratkevich S V 2012 *J. Nanophotonics* **6** 061712
[262] Poklonski N A, Kislyakov E F and Vyrko S A 2013 Electromechanical vibrator based on graphene *Proc. of Int. Conf. Shell and Membrane Theories in Mechanics and Biology: from Macro- to Nanoscale Structures, Minsk, 16–20 Sept. 2013* ed G I Mikhasev and H Altenbach (Minsk: BSU) pp 105–8
[263] Kleshch V I, Obraztsov A N and Obraztsova E D 2010 *Carbon* **48** 3895–900
[264] Zandiatashbar A, Lee G H, An S J, Lee S, Mathew N, Terrones M, Hayashi T, Picu C R, Hone J and Koratkar N 2014 *Nat. Commun.* **5** 3186
[265] Han M Y, Brant J C and Kim P 2010 *Phys. Rev. Lett.* **104** 056801
[266] Sprinkle M, Ruan M, Hu Y, Hankinson J, Rubio-Roy M, Zhang B, Wu X, Berger C and de Heer W A 2010 *Nat. Nanotechnol.* **5** 727–31
[267] Baringhaus J *et al* 2014 *Nature* **506** 349–54
[268] Lusk M T and Carr L D 2008 *Phys. Rev. Lett.* **100** 175503
[269] Yazyev O V and Louie S G 2010 *Phys. Rev.* B **81** 195420
[270] Zhang T, Li X and Gao H 2014 *J. Mech. Phys. Solids* **67** 2–13
[271] da Silva C A B, Correa S M, dos Santos J C da S, Nisioka K R, Moura-Moreira M, Wang Y P, Del Nero J and Cheng H P 2018 *J. Appl. Phys.* **124** 084303

[272] Ewels C P, Rocquefelte X, Kroto H W, Rayson M J, Briddon P R and Heggie M I 2015 *Proc. Natl. Acad. Sci. USA* **112** 15609–12
[273] Krishnan A, Dujardin E, Treacy M M J, Hugdahl J, Lynum S and Ebbesen T W 1997 *Nature* **388** 451–4
[274] Terrones H 1994 *J. Math. Chem.* **15** 143–56
[275] Balaban A T, Klein D J and Liu X 1994 *Carbon* **32** 357–9
[276] Charlier J C and Rignanese G M 2001 *Phys. Rev. Lett.* **86** 5970–3
[277] Naess S N, Elgsaeter A, Helgesen G and Knudsen K D 2009 *Sci. Technol. Adv. Mater.* **10** 065002
[278] Jaszczak J A, Robinson G W, Dimovski S and Gogotsi Y 2003 *Carbon* **41** 2085–92
[279] Iijima S, Yudasaka M, Yamada R, Bandow S, Suenaga K, Kokai F and Takahashi K 1999 *Chem. Phys. Lett.* **309** 165–70
[280] Ajima K, Yudasaka M, Murakami T, Maigné A, Shiba K and Iijima S 2005 *Mol. Pharm.* **2** 475–80
[281] Yoshitake T *et al* 2002 *Physica* B **323** 124–6
[282] Cano-Marquez A G *et al* 2015 *Sci. Rep.* **5** 10408
[283] Poklonski N A, Vyrko S A and Vlassov A T 2009 Regular-block modeling of clusters in the carbon arc discharge plasma *Contributed Papers of VI Int. Conf. Plasma Physics and Plasma Technology (PPPT-6), Minsk, 28 Sept.–2 Oct. 2009* vol II (Minsk: Polyfact) pp 740–3
[284] Kolesnikov D V and Osipov V A 2009 *Phys. Part. Nuclei* **40** 502–24
[285] Jiang D and Chen Z (ed) 2013 *Graphene Chemistry: Theoretical Perspectives* (Chichester: Wiley)
[286] Winston R, Miñano J C, Benítez P and Welford W T 2005 *Nonimaging Optics* (Amsterdam: Elsevier Academic Press)
[287] Seisyan R P 2005 *Tech. Phys.* **50** 535–45
[288] Ershova O V, Lozovik Y E, Popov A M, Bubel' O N, Kislyakov E F, Poklonskii N A, Knizhnik A A and Lebedeva I V 2008 *JETP* **107** 653–61
[289] Poklonski N A, Vlassov A T and Vyrko S A 2013 Model of cantilever made of carbon surface *Proc. of Int. Conf. Shell and Membrane Theories in Mechanics and Biology: from Macro- to Nanoscale Structures, Minsk, 16–20 Sept. 2013* ed G I Mikhasev and H Altenbach (Minsk: BSU) pp 95–8 [in Russian]
[290] Lavrik N V, Sepaniak M J and Datskos P G 2004 *Rev. Sci. Instrum.* **75** 2229–53
[291] Poklonski N A, Kislyakov E F, Vyrko S A and Ratkevich S V 2015 Electromechanical generator: going from micro to nano size *Physics, Chemistry and Applications of Nanostructures. Reviews and Short Notes: Proc. of Int. Conf. Nanomeeting-2015, Minsk, 26–29 May 2015* ed V E Borisenko *et al* (Singapore: World Scientific) pp 613–6
[292] Poklonski N A, Kislyakov E F, Sagaidak D I, Siaglo A I and Fedoruk G G 2001 *Tech. Phys. Lett.* **27** 180–2
[293] Walzer K and Hietschold M 2001 *Surf. Sci.* **471** 1–10
[294] Baran J D and Larsson J A 2010 *Phys. Chem. Chem. Phys.* **12** 6179–86
[295] Nizovtsev A S and Kozlova S G 2013 *J. Phys. Chem.* A **117** 481–8
[296] Wang Y, Kröger J, Berndt R and Hofer W A 2009 *J. Am. Chem. Soc.* **131** 3639–43
[297] Poklonski N A, Vyrko S A, Ratkevich S V and Siahlo A I 2017 Inversion of the SnPc molecule on graphene *Physics, Chemistry and Applications of Nanostructures. Reviews and Short Notes: Proc. of Int. Conf. Nanomeeting-2017, Minsk, 30 May–2 June 2017* ed V E Borisenko *et al* (Singapore: World Scientific) pp 65–8
[298] Xie X, Ju L, Feng X, Sun Y, Zhou R, Liu K, Fan S, Li Q and Jiang K 2009 *Nano Lett.* **9** 2565–70
[299] Kim J H and Benelmekki M 2016 *ACS Appl. Mater. Interfaces* **8** 33121–30
[300] Chen Y, Lu J and Gao Z 2007 *J. Phys. Chem.* C **111** 1625–30
[301] Pan H, Feng Y and Lin J 2005 *Phys. Rev.* B **72** 085415
[302] Mpourmpakis G, Tylianakis E and Froudakis G E 2007 *Nano Lett.* **7** 1893–7
[303] Coluci V R, Braga S F, Baughman R H and Galvão D S 2007 *Phys. Rev.* B **75** 125404
[304] Braga S F, Coluci V R, Legoas S B, Giro R, Galvão D S and Baughman R H 2004 *Nano Lett.* **4** 881–4
[305] Zheng B and Gao C 2016 *New Carbon Mater.* **31** 315–20
[306] Zheng B, Xu Z and Gao C 2016 *Nanoscale* **8** 1413–20
[307] Guo Y, Zhao G, Wu N, Zhang Y, Xiang M, Wang B, Liu H and Wu H 2016 *ACS Appl. Mater. Interfaces* **8** 34185–93
[308] Shi X, Pugno N M and Gao H 2010 *J. Comput. Theor. Nanosci.* **7** 517–21
[309] Shi J, Yin H, Yu J, Liu L and Cai K 2016 *Comput. Mater. Sci.* **125** 146–53
[310] Savin A V, Korznikova E A and Dmitriev S V 2015 *Phys. Rev.* B **92** 035412
[311] Siahlo A I, Poklonski N A, Lebedev A V, Lebedeva I V, Popov A M, Vyrko S A, Knizhnik A A and Lozovik Y E 2018 *Phys. Rev. Materials* **2** 036001
[312] Siahlo A I, Poklonski N A, Vyrko S A and Ratkevich S V 2018 *Semiconductors* **52** 1886–9
[313] Lin Y M, Jenkins K A, Valdes-Garcia A, Small J P, Farmer D B and Avouris P 2009 *Nano Lett.* **9** 422–6
[314] Cheng R, Bai J, Liao L, Zhou H, Chen Y, Liu L, Lin Y C, Jiang S, Huang Y and Duan X 2012 *Proc. Natl. Acad. Sci. USA* **109** 11588–92
[315] Lin Y M *et al* 2011 *Science* **332** 1294–7
[316] Zheng J, Wang L, Quhe R, Liu Q, Li H, Yu D, Mei W N, Shi J, Gao Z and Lu J 2013 *Sci. Rep.* **3** 1314
[317] Zhang Z, Zou X, Xu L, Liao L, Liu W, Ho J, Xiao X, Jiang C and Li J 2015 *Nanoscale* **7** 10078–84
[318] Gao N, Gao T, Yang X, Dai X, Zhou W, Zhang A and Lieber C M 2016 *Proc. Natl. Acad. Sci. USA* **113** 14633–8
[319] Blaschke B M, Lottner M, Drieschner S, Bonaccini Calia A, Stoiber K, Rousseau L, Lissourges G and Garrido J A 2016 *2D Mater.* **3** 025007
[320] Poklonski N A, Siahlo A I, Vyrko S A, Popov A M, Lozovik Y E, Lebedeva I V and Knizhnik A A 2013 *J. Comput. Theor. Nanosci.* **10** 141–6
[321] Popov A M, Lebedeva I V, Knizhnik A A, Lozovik Y E, Potapkin B V, Poklonski N A, Siahlo A I and Vyrko S A 2013 *J. Chem. Phys.* **139** 154705
[322] Kats E I 2015 *Phys. Usp.* **58** 892–6
[323] Lebedeva I V, Popov A M, Knizhnik A A, Lozovik Y E, Poklonski N A, Siahlo A I, Vyrko S A and Ratkevich S V 2015 *Comput. Mater. Sci.* **109** 240–7
[324] Ng K K 2002 *Complete Guide to Semiconductor Devices* (New York: Wiley-IEEE Press)
[325] González J W, Santos H, Pacheco M, Chico L and Brey L 2010 *Phys. Rev.* B **81** 195406
[326] Berahman M, Sanaee M and Ghayour R 2014 *Carbon* **75** 411–9
[327] Luryi S 1988 *Appl. Phys. Lett.* **52** 501–3
[328] Luryi S 1991 *Appl. Phys. Lett.* **59** 2335–6
[329] Hwang H J and Kang J W 2014 *Physica* E **56** 17–23
[330] Kang J W, Park J and Kwon O K 2014 *Physica* E **58** 88–93
[331] Zheng Q, Jiang B, Liu S, Weng Y, Lu L, Xue Q, Zhu J, Jiang Q, Wang S and Peng L 2008 *Phys. Rev. Lett.* **100** 067205

[332] Siahlo A I, Popov A M, Poklonski N A, Lozovik Y E, Vyrko S A and Ratkevich S V 2016 *Physica* E **84** 348–53
[333] Greenberg Y S, Pashkin Y A and Il'ichev E 2012 *Phys. Usp.* **55** 382–407
[334] Todorović D, Matković A, Milićević M, Jovanović D, Gajić R, Salom I and Spasenović M 2015 *2D Mater.* **2** 045013
[335] Lee J and Novikov N (ed) 2004 *Innovative Superhard Materials and Sustainable Coatings for Advanced Manufacturing* (Dordrecht: Springer)
[336] Takahashi K, Yoshikawa A and Sandhu A (ed) 2007 *Wide Bandgap Semiconductors: Fundamental Properties and Modern Photonic and Electronic Devices* (Dordrecht: Springer)
[337] Metcalfe A, Fern G R, Hobson P R, Smith D R, Lefeuvre G and Saenger R 2017 *JINST* **12** C01066
[338] Blank V D *et al* 1999 *Diamond Relat. Mater.* **8** 1285–90
[339] Karkin A E, Voronin V I, Berger I F, Kazantsev V A, Ponosov Y S, Ralchenko V G, Konov V I and Goshchitskii B N 2008 *Phys. Rev.* B **78** 033204
[340] Poklonski N A, Lapchuk T M, Gorbachuk N I, Nikolaenko V A and Bachuchin I V 2005 *Semiconductors* **39** 894–7
[341] Wang K, Steeds J W, Li Z and Wang H 2017 *Appl. Phys. Lett.* **110** 152101
[342] Ekimov E A and Kondrin M V 2017 *Phys. Usp.* **60** 539–58
[343] Doherty M W, Manson N B, Delaney P, Jelezko F, Wrachtrup J and Hollenberg L C L 2013 *Phys. Rep.* **528** 1–45
[344] Chunnilall C J, Degiovanni I P, Kück S, Müller I and Sinclair A G 2014 *Opt. Eng.* **53** 081910
[345] Klemencic G M, Mandal S, Werrell J M, Giblin S R and Williams O A 2017 *Sci. Technol. Adv. Mater.* **18** 239–44
[346] Okazaki H, Wakita T, Muro T, Nakamura T, Muraoka Y, Yokoya T, Kurihara S, Kawarada H, Oguchi T and Takano Y 2015 *Appl. Phys. Lett.* **106** 052601
[347] Bennet K E *et al* 2016 *Front. Hum. Neurosci.* **10** 102
[348] Kaiser W and Bond W L 1959 *Phys. Rev.* **115** 857–63
[349] Kiflawi I, Mayer A E, Spear P M, Van Wyk J A and Woods G S 1994 *Phil. Mag.* B **69** 1141–7
[350] Abbaschian R, Zhu H and Clarke C 2005 *Diamond Relat. Mater.* **14** 1916–9
[351] Khmelnitskii R A 2015 *Phys. Usp.* **58** 134–49
[352] Rebrov A K 2017 *Phys. Usp.* **60** 179–86
[353] Poklonski N A 2006 *Tech. Phys. Lett.* **32** 309–11
[354] Kessenikh A V 2009 *Phys. Usp.* **52** 695–722
[355] Alshits V I, Darinskaya E V, Koldaeva M V, Kotowski R K, Petrzhik E A and Tronczyk P 2017 *Phys. Usp.* **60** 305–18
[356] Collins A T 2002 *J. Phys.: Condens. Matter* **14** 3743–50
[357] Smith W V, Sorokin P P, Gelles I L and Lasher G J 1959 *Phys. Rev.* **115** 1546–52
[358] Poklonski N A, Vyrko S A, Poklonskaya O N, Lapchuk N M and Munkhtsetseg S 2013 *J. Appl. Spectrosc.* **80** 366–71
[359] Poklonski N A, Lapchuk N M and Lapchuk T M 2004 *JETP Lett.* **80** 748–51
[360] Poklonskii N A, Lapchuk T M, Baev V G and Gusakov G A 2006 *J. Appl. Spectrosc.* **73** 5–9
[361] Poklonski N A, Lapchuk N M, Khomich A V, Lu F X, Tang W Z, Ralchenko V G, Vlasov I I, Chukichev M V and Sambuu M 2007 *Chin. Phys. Lett.* **24** 2088–90
[362] Kazuchits N M, Rusetsky M S, Kazuchits V N and Zaitsev A M 2016 *Diamond Relat. Mater.* **64** 202–7
[363] Poklonski N A, Kislyakov E F, Bubel O N and Vyrko S A 2011 Maser effect in a Jahn–Teller center: Single substitutional nitrogen atom in diamond *Physics, Chemistry and Applications of Nanostructures. Reviews and Short Notes: Proc. of Int. Conf. Nanomeeting-2011, Minsk, 24–27 May 2011* ed V E Borisenko *et al* (Singapore: World Scientific) pp 110–3
[364] Breeze J D, Salvadori E, Sathian J, Alford N M and Kay C W M 2018 *Nature* **555** 493–6
[365] Aharonovich I, Castelletto S, Simpson D A, Su C H, Greentree A D and Prawer S 2011 *Rep. Prog. Phys.* **74** 076501
[366] Dobrinets I A, Vins V G and Zaitsev A M 2013 *HPHT-Treated Diamonds: Diamonds Forever* (Berlin: Springer)
[367] Lohrmann A, Pezzagna S, Dobrinets I, Spinicelli P, Jacques V, Roch J F, Meijer J and Zaitsev A M 2011 *Appl. Phys. Lett.* **99** 251106
[368] Wilson A H 1980 *Proc. R. Soc. London Ser.* A **371** 39–48
[369] Peierls R 1980 *Contemp. Phys.* **21** 3–17
[370] Malinovskii V K 1999 *Phys. Solid State* **41** 725–8
[371] Shevchenko V Y 2012 *Struct. Chem.* **23** 1089–101
[372] Poklonski N A 2016 *Science and Innovations (NASB)* **No. 8** 64–9 http://innosfera.by/files/2016/8.pdf [in Russian]
[373] Singh V, Joung D, Zhai L, Das S, Khondaker S I and Seal S 2011 *Prog. Mater. Sci.* **56** 1178–271
[374] Rao R *et al* 2018 *ACS Nano.* **12** 11756–84
[375] Clancy A J, Bayazit M K, Hodge S A, Skipper N T, Howard C A and Shaffer M S P 2018 *Chem. Rev.* **118** 7363–408
[376] Ratnikov P V and Silin A P 2018 *Phys. Usp.* **61** 038231
[377] Bukharaev A A, Zvezdin A K, Pyatakov A P and Fetisov Y K 2018 *Phys. Usp.* **61** 038279